Science
AAAS

Supplementary Materials for

Ecosystem fluxes during drought and recovery in an experimental forest

Christiane Werner *et al.*

Corresponding author: Christiane Werner, c.werner@cep.uni-freiburg.de

Science **374**, 1514 (2021)
DOI: 10.1126/science.abj6789

The PDF file includes:

Materials and Methods
Figs. S1 to S9
Tables S1 to S8
References

Materials and Methods

Tropical Rainforest Mesocosm

The Biosphere 2 (B2) Tropical Rainforest (TRF) is a large-scale (27,700 m^3/1940 m^2) fully enclosed (glass-steel-concrete) mesocosm (Fig. S1-S3) near Tucson, AZ, USA containing a phylogenetically diverse assemblage of pan-tropical plant species (*37, 38*) with established (30-year old) interactions among the model ecosystem's pedosphere, hydrosphere, and atmosphere. The mesocosm is uniquely suited for controlled ecosystem-scale experiments that manipulate climate and atmospheric composition, precisely introduce tracers including stable isotope labeling, and capture processes across plot to ecosystem scales (*20, 39*). The tropical rainforest is particularly well-suited for drought and rewet experiments (*20, 40–43*) because climate and hydrological inputs (rain, groundwater) are directly controlled. The structural features of the system allow unparalleled access to ecosystem components for monitoring and sampling (e.g., soil subsurface, ecosystem drainage, canopy access). Due to these features, the mesocosm can be seen as a large-scale cuvette to quantify net ecosystem exchange of energy and biogeochemical variables.

The forest is distributed across a topographically rich landscape rooted in 2-4 m of soil (sandy clay loam: 20–35 % clay and >70 % sand) underlain by an impervious concrete and steel floor with a piped drainage system (*38, 44*). Climate conditions are controlled to broadly reflect Earth's tropical rainforests. Overhead sprinklers deliver precipitation without strong seasonality. The precipitation regime is three times a week for approximately 1600 mm/year, unless drought experiments are conducted (*42*). TRF temperatures (~32 °C on average) are warmer than Earth's tropical rainforests and vary seasonally with solar radiation in southern Arizona. Further, the glass enclosure establishes a stronger temperature inversion and lower VPD (under non-drought conditions) relative to external sites. Incoming solar radiation is reduced by approximately 40 %, and no radiation wavelengths below 385 nm pass through the mylar sheet in the glass panels (*45*). Due to this UV-screening glass, atmospheric oxidation effects are negligible and atmospheric VOC concentrations reflect the interplay between vegetation emissions and net exchange rates with soil (Fig. 1E, F). Overall, the well-developed TRF model ecosystem demonstrates broadly similar behavior to the world's tropical rainforests (*20*). It serves as a valuable model system to rigorously evaluate tropical ecosystem responses to warmer and hydrologically more variable climates.

We selected most dominant canopy forming tree species in the rainforest representing approximately 70% crown coverage. In particular, we choose all dominant species with sufficient replicates (n = 4-5, *Clitoria fairchildiana* R. A. Howard - CF, *Pachira aquatica* Aubl.- PA, *Phytolacca dioica* L.- PD), beside three palm trees. Further we also included large individuals that contributed a significant part of the canopy (*Ceiba pentandra* (L.) Geartn- CP, *Hibiscus tilliaceus* L.- HT, *Hura crepitans* L.- HC), representing approximately 10% crown cover. For the understory, we selected representative species regarding their abundance and total cover (ca. 50 %, for species list see Table S1).

Controlled Ecosystem Drought

The B2-WALD campaign started in September 2019 with a pre-drought phase, followed by early drought, severe drought, and recovery periods (Fig. S4). The ecosystem was generally maintained within a temperature range between 21 and 37 °C (day) and 20 and 27 °C (night) (Table S5) using air handling units (AHUs) and ventilation as needed. Ecosystem water content was manipulated with moisture addition (rain sprinklers or deep water) and removal (condensation and ventilation).

Ecosystem moisture manipulation began with turning off aesthetic water features (waterfall, stream, pond) before the experiment (31 May 2019) to ensure timely drought progress during the campaign. The forest was monitored for 36 days under pre-drought conditions with a rainfall regime of ~30 mm per week or ~1,600 mm per year. The early drought started on 8 October 2019 following the final rain (midnight 7 October 2019). During the severe drought (1 November 2019 to 2 December 2019), relative humidity was actively reduced using a large AHU, which first cooled the air leading to condensation, and then re-heated it to maintain temperature. During this period, a persistent water table in the isolated drainage basin of the Varzea sub habitat (Fig. S2) was manually drained to enhance drought conditions (12 November 2019). Water was not added to the system for 55 days (8 October 2019 to 2 December 2019) and the ecosystem went 65 days (8 October 2019 to 12 December 2019) without rain (Fig. S4). These moisture manipulations represented the second most extreme drought imposed on the B2 tropical rain forest. Of the eight prior droughts, only the one in 2014 (*42*) was more severe.

The forest was first rewet from below by adding a total amount of ~23,000 L of ^{2}H-labeled water to the subsurface drainage network over a four-day period spanning 2 to 5 December 2019 (see *Ecosystem-Scale Isotope Labeling*). The ecosystem response to the addition of water at the base of the ecosystem was monitored for 10 days, during which surface conditions continued to reflect severe drought. The end of the drought period was initiated with

a rainfall event at 11:00 on 12 December 2019 (~35,000 L or ~18 mm). The second rainfall was conducted one week later (11:00 on 19 December, ~36,000 L or ~19 mm) and subsequent rain events occurred every second day beginning at 00:00 on 21 December. In all subsequent rain events, ~10 mm (20,000 L) of water was added to the system over a 4.5-hour period. Rainfall was added on a quadrant-by-quadrant basis in 15-min periods.

Ecosystem-Scale Isotope Labeling

Stable isotope labeling was performed at a whole-ecosystem scale at three time points during the B2-WALD campaign: (1) atmosphere $^{13}CO_2$ labeling during pre-drought, (2) atmosphere $^{13}CO_2$ labeling during severe drought and (3) deep-water ^{2}H labeling in the latest part of the severe drought (Fig. S4).

99 atom % $^{13}CO_2$ from gas tanks (Sigma Aldrich, St. Louis MO, USA) was released into the atmosphere at two ground-based locations at 8:00 on 5 October 2019 (pre-drought: 150 L, maximum $\delta^{13}C$ value at 20 m = +1183 ± 4 ‰, Vienna Pee Dee Belemnite (VPDB)) and at 9:00 on 22 November 2019 (severe drought: 300 L, maximum $\delta^{13}C$ value at 20 m = +2541 ± 222 ‰, VPDB), where the reported standard deviations (of 2-min averages) reflect rapid changes in atmospheric $\delta^{13}C$ values during pulse labeling, especially during the second, stronger labeling. The $^{13}CO_2$ was rapidly mixed throughout the ecosystem by the fans and was widely distributed within ~20 minutes. The atmosphere remained sealed for 4.0 and 5.2 hours during the first and second labeling periods, respectively. To return to background $\delta^{13}C$ values of atmospheric CO_2 after labeling, the ecosystem was flushed by reinstating outside air ventilation and opening the windows of the rainforest for 4.3 and 5.2 hours following the first and second labeling periods, respectively. The longer and stronger labeling during drought was designed to ensure a similar ecosystem ^{13}C uptake as in pre-drought, even though assimilation rates were lower under drought (Fig. 1). A correspondingly longer ventilation period was required to flush the stronger label following this second labeling event.

Simultaneous to the pulse labeling, a second CO_2 line was added to the gas-mixing manifold to deliver ^{13}C-labeled CO_2 (10 atom % ^{13}C, P/N 600180, MilliporeSigma, Burlington MA, USA) to leaf chambers (see *Leaf measurements*) to match the atmospheric $^{13}CO_2$ enrichment. The amount of CO_2 added from the normal 5 % CO_2 tank source was meanwhile reduced to maintain typical leaf chamber total CO_2 concentrations (for further details of the gas sampling system, see *Composition and Gas Exchange of Ecosystem Compartments*).

Deep water enriched in ^{2}H was added in the final phase of severe drought (see *Controlled Ecosystem Drought*). 14,000 L ($\delta^{2}H$ ~ 3000 ‰, Vienna Standard Mean Ocean Water (VSMOW)) were pumped into the soil via the subsurface drainage network (along the steel/concrete base of the enclosed system) and an additional 9,000 L ($\delta^{2}H$ ~ 1500 ‰, VSMOW) were added at the bottom of vertical 6” PVC pipes and soil pits to the base of the ecosystem to ensure an even distribution of ^{2}H-labeled deep water.

Destructive sampling

Throughout the campaign leaf and root material was sampled to monitor leaf water potential (LWP) and to track carbon allocation through the system.

Leaf water potential

A total of nine plant species were monitored for leaf water potential, with six of the species having multiple replicates (see Table S1, S6 for species selection and grouping). Care was taken to select 1) proper leaf dimension for leaf water potential to be accurately determined using a Scholander type pressure chamber (PMS Instrument Company, OR, USA) (*46*), 2) spatial location within the rainforest biome, and 3) compatibility with other data collection goals of the B2-WALD campaign.

Predawn (pLWP) and midday water potential (mLWP) measurements were conducted throughout the experiment, with both pLWP and mLWP measured during the dry-down/drought phase (25 October 2019, 1 November 2019, 8 November 2019, 15 November 2019, 24 November 2019), deep re-wet (3 December 2019, 6 December 2019), and recovery (13 December 2019, 20 December 2019). Additional pLWP measurements were conducted on 1 October 2019 and additional mLWP were conducted on 23 August 2019, 25 September 2019, and 1 December 2019. To adjust for later sunrise, pLWP was measured at 05:30 in August and at 06:30 by December. mLWP measurements were made from 10:00 to 11:00, since previous studies from the tropical forest biome have found that plant activity decreases after 11:00, when temperatures increase in the biome (*20*). Late morning mLWP measurements allowed us to sample leaves at the most negative water potential values. For both predawn and midday WP measurements, all leaves were collected within 30 minutes by climbers ascending into the rainforest canopy. Typically, large branches were collected in the canopy from which small twigs with 3-5 leaves were measured. In instances when whole branches were not collected, cut leaves were placed into ziplock bags and sealed until measurement (within 5 minutes).

Leaf sampling

To track assimilation of C into leaf tissue during the pre-drought and drought period we collected fresh leaf matter from representative species (Table S6). We collected leaves within the week before each $^{13}CO_2$-pulse and then 0, 1, 3, and 5 days after the labeling. On each sampling day, we collected leaves during a 30-minute window in the late morning, when assimilation in the TRF is highest (*20*). Leaves were transferred to 50 mL plastic tubes and immediately frozen in liquid nitrogen or dry ice to stop metabolic activity. All leaf samples were stored at -20 °C until further processing.

Leaf $\delta^{13}C$ analysis

Leaf samples were freeze-dried at the University of Arizona and sent to the Max Planck Institute for Biogeochemistry (Jena, Germany) for isotopic analysis. Samples were ground to fine powder using a ball mill (Retsch® MM400, Haan, Germany). Approximately 0.1 mg of ground material was weighed into tin cups and analyzed with a Finnigan Delta Plus XL EA-IRMS (Thermo Finnigan GmbH, Bremen, Germany) coupled to an autosampler. For every 20-25 samples, approximately 5-7 standards (acetanilide, -30.06 ‰) were measured to reference the samples to the VPDB scale with a single point calibration. The precision of the $\delta^{13}C$ measurements of the acetanilide standard was < 0.16 ‰ (1 σ). Caffeine (-40.46 ‰) was also measured as a quality control after every 25 samples, and was always within 0.2 ‰ of its known value.

Root sampling

To collect fine root samples, soil cores were collected at six representative locations throughout the rainforest ecosystem (Fig. S2b; near all four pit locations P1–4 and two additional root sampling sites). Of those sampling locations, four sites (Sites 1-4) were paired with the automatic soil chamber locations, all of which were adjacent to tall tree species (see *Composition and gas exchange of ecosystem compartments, Soil fluxes*). The additional sampling sites (Sites 5 and 7) were in locations dominated by understory plants. Cores were collected seven times between 1 October 2019 and 11 December 2019 from four randomized positions within each of the six sites. The seven sampling dates included one pre-label sampling (1 October 2019) and three sampling points within 30 days following each of the two $^{13}CO_2$ pulses.

Cores were collected with a manual root auger (8 cm diameter), immediately separated into three depth increments (0-15 cm, 15-30 cm and 30-50 cm), transferred into clean plastic bags and cooled to 4 °C. Within three days, fine roots were carefully removed from each sample manually with tweezers.

Root processing and $\delta^{13}C$ analysis

Fine root biomass was freeze-dried in paper bags, dry weight per soil increment was measured, and the biomass was finely ground in a ball mill. Approximately 0.5-1 mg of root material was weighed into tin capsules to prior to measuring $\delta^{13}C$ values with a Costech ECS 4010 elemental analyzer (CostechAnalytical Technologies Inc. Valencia, USA) coupled by a ConFlo III interface to a Delta C IRMS (both units from Thermo Fisher Scientific, Bremen, Germany) at the Center of Stable Isotope analysis (KOSI, Goettingen, Germany). For every 8 samples, 2 standards (acetanilide, -29.73 ‰) were measured to reference $\delta^{13}C$ measurements to the VPDB scale with a single point calibration. The precision of the acetanilide standard was < 0.05‰ (1 σ).

Environmental sensors

Environmental conditions in the B2 TRF were monitored along four above and below ground sensor profiles (Fig. S2, S3). The four profile locations were chosen to represent the complete vertical gradient and main forest areas.

Above ground sensor profiles

Sensors were located at 1, 3, 7, 13, and (only S and NE towers) 20 m height above the soil surface (Fig. S3). At each level we measured photosynthetic active radiation (PAR) (Apogee SQ110, Campbell Scientific, Logan, UT, USA), temperature, and relative humidity with Vaisala HMP 45c sensors (Vaisala Oyi., Vantaa, Finland), housed in a naturally-aspirated solar radiation shield (Campbell Scientific 41003-5, Logan, UT, USA). All sensors were re-calibrated in Spring 2019 either by factory calibration (light and wind sensors and some temperature/humidity sensors) or cross-calibrated to factory-calibrated sensors.

From the temperature (T) and relative humidity (RH), we calculated the vapor pressure deficit (VPD in kPa) based on the saturated vapor pressure equation:

$$VPD = 0.6108\left(1 - \frac{RH}{100}\right)e^{\frac{17.27T}{(237.3+T)}}$$

VPD values were averaged per height zone (H1-5) as shown in Fig. S3. Zones H1 and H2 were considered representative of the understory, while Zone H4 was considered representative of the canopy conditions (as median height of the canopy).

We measured the CO_2 concentration in three different heights (1, 13, and 27 m above the soil surface, Fig. S3) using Vaisala GMP 343 sensors (Vaisala Oyi., Vantaa, Finland). The sensors reported the one-minute averaged CO_2 concentration every 15 minutes. Prior to mounting, the CO_2 sensors were calibrated to four NOAA CO_2 standard tanks (ranging from 300 to 500 ppm CO_2). For carbon budget calculations, we divided the rainforest profile into three height zones (C1-3, see Fig. S3)

Air pressure was measured with two WeatherHawk 520 stations (Vaisala Oyi., Vantaa, Finland) in a central location in the rainforest (~2 m height along the NE tower, from the start of the experiment until 31 October 2019) and across one of the AHUs in the basement (AHU#1 from 31 October 2019 until the end of the experiment). We placed the WeatherHawks in the central part of the AHU inlet and outlet to measure wind speed, direction, air pressure, humidity and temperature. The units were cross-calibrated before installation across the AHU (at ~1.5 m height on the NE tower). WeatherHawk data were reported at one-minute intervals on a CR1000x using an SDI-12 protocol.

Below ground sensor profiles

Four soil pits (0.9 x 1.5 m) spanning the vertical distance from soil surface to the concrete sub-surface underlying the soil (bottom depths: P1 = 180 cm, P2 = 310 cm, P3 = 290 cm, P4 =200 cm) were installed (P1, P3, and P4 in 2010 and 2011; P2 in Summer 2019) at different locations across the rainforest ecosystem (Fig. S2). Aluminum casing and plexiglass windows were used to stabilize soil pit walls. The soil was accessible via holes within the plexiglass (10 cm diameter), which were used to install and maintain sensors throughout the experiment. Only sensors in 5 cm soil depth were installed from the soil surface. In July 2019, soil moisture and temperature sensors (output VWC m^3 m^{-3} and T ºC SMT100, Truebner Gmbh, Neustadt, Germany) and soil water potential sensors (output WP kPa and T °C TEROS 21, Meter Group, Pullman, WA, USA) were installed in all four pits at 5, 10, and 20 cm depth. The SMT100 sensors were also installed at 50, 100, 200 cm (for pits deeper than 2 m), and right above the surface of the concrete.

Soil water potential (WP) for the shallow soil was calculated based on the average of the 5 and 10 cm TEROS 21 probes from all four pits. The deep soil WP was calculated based on the soil moisture measurements at the bottom of each soil pit and the water retention curve for gravel-soil mixtures. Gravel content and soil parameters were based on soil texture analysis from at least three samples per pit.

Tree stem moisture content measurements

To continuously measure the water content and subsequently quantify the total amount of water stored in tree xylem, we inserted a total of 11 time-domain reflectometers (10 and 15 cm needle length; TDR, 310H and 315H, Acclima Inc., Meridian, ID, USA) at ~1.3 m height into the stems of predominantly the upper canopy tree species (Table S6), but also two understory trees (PA2 and PA3). CF individuals commonly consisted of multiple stems. For CF3, sensors were installed in the two main stems (CF3a and CF3b). To install the probes, a drill-guide was strapped to the tree and ⅛" holes were carefully drilled into the stem. The probes were then lubricated with wood polish (Howard Feed-N-Wax, Howard Products Inc, Paso Robles, USA) and inserted into the stems. The TDR probe data output included the volumetric water content (VWC m^3 m^{-3}) and the housing temperature. The 315H sensors, featuring longer needles of 15 cm length, were installed in the trees with the largest DBH (CF3a, CP, HC, HT, PA4, and PD1) (Tables S1; S6).

Sap flow measurements

To quantify water transported in tree xylem, a total of 16 heat-pulse velocity sap flow sensors (HPV-06, Implexx Sense, Edaphic Scientific, Melbourne, Australia) were installed in individuals of seven different species (Table S6). The installation height was 110-130 cm above ground for all trees except HR, which were shrub individuals with multiple small stems. HR sensors were installed at 10-40 cm above ground. Both CF3 and CF4 were equipped with two sap flow sensors (CF3a,b and CF4a,b) to evaluate variability between their multiple stems. For individuals with a bark depth > 0.6 cm, bark was removed to ensure the location of the outer measuring point within conductive sap wood. Similar to the TDR probes, a drilling guide was strapped to the tree trunk, holes were drilled, sensor needles were lubricated with wood polish and pushed inside predrilled holes. Finally, sensors were insulated on the outside to reduce the impact of air temperature variations on measurements.

We calculated tree sap flux density (V_s in cm hr^{-1}) from the raw sap flow sensor output according to (*47*):

$$V_s = \frac{V_h' \rho_b (C_w + mC_s)}{\rho_s C_s}$$

where V_h' is the measured sap flux velocity corrected for wounding and probe misalignment (zero offset), ρ_b and ρ_s are wood (Table S1) and sap (1000 kg m^{-3}) density, respectively; C_w and C_s are the specific heat capacities of dry wood (1200 $Jg^{-1}\ ^oC^{-1}$) and sap (4182 $J\ g^{-1}\ ^oC^{-1}$), respectively; and *m* is the moisture content of sapwood (derived from the stem moisture measurements with the TDR probes). The whole tree sap flux (Q,L,d^{-1}) was then calculated based on the tree radius and V_s for both the outer and inner measurement location (0.5-1.5 and 1.5-2.5 cm into the tree), the knowledge that sap fluxes decrease with depth in the tree (*48-50*), and that we observed no change from sapwood to heartwood in the cores from any of the trees we measured.

The calculations were based on the tree radius (to closest integer value not including bark (estimated to be ~0.5 cm deduction)/sap-flowing radius and V_s for both the inner and outer measurement location (*48-50*):

$$Q = \frac{(\pi(r^2 - (r-1)^2)V_s^O + \pi((r-1)^2 - (r-2)^2)V_s^I) + \sum_{i=2}^{i=r-1} \pi((r-i)^2 - (r-i-1)^2) * \begin{cases} If\ RV_h' > 1\ then\ V_s^I \frac{1}{(RV_h')^i} \\ If\ RV_h' < 1\ then\ V_s^I (RV_h')^i \end{cases}}{1000}$$

where r stands for the stem radius and the numerical subtractions denote the reduction in radius based on a 1cm measurement width for each of the thermistors. V_s^O and V_s^I stand for the calculated outer and inner sap flux velocity and RV_h' for the ratio of the measured outer and inner sap velocity V_h^O/V_h^I.

Finally, we summed the total tree water fluxes (TWF) from the individual measured stems for the total water flux changes shown in Fig. 1. Since the measured trees are only about one third of the total TRF tree population, we presume even the total Q water flux to be a severe underestimation of the total TRF water flux.

Ecosystem Calculations

Exchange rate measurements

Air exchange rates (ER) of the Biosphere 2 rainforest ecosystem with the outside air represent the biome's atmospheric residence time when (normally) operated in flow-through mode and the leak rate through the glass and steel enclosure when (infrequently) operated in closed mode. We measured ER with a conserved, purely man-made tracer (sulfur hexafluoride, SF_6) 187 times during the experiment. For each measurement, 25 to 30 mL SF_6 were injected into the rainforest to generate a concentration of ~1 ppb (~125 times background air at ~8 ppt). The SF_6 was sampled next to the instrument laboratory with a single, filtered inlet connected to ¼" OD Teflon tubing. SF_6 concentration was measured on a SRI Greenhouse Gas GC (SRI Instruments, Torrance, CA, USA) with an automated sample loop of 1 ml using an ECD detector at 350 °C. SF_6 in the sample and carrier UHP N_2 stream was separated from N_2O using a Hayesep D column at 65 °C. Each sample was collected and analyzed every 2.5 minutes. The exchange rate was calculated for the exponential decay of the SF_6 concentration in the Biosphere 2 rainforest and reported as % per hour.

Ecosystem Carbon Cycling

Net Ecosystem Exchange (NEE) is the exchange of carbon dioxide (CO_2) between the atmosphere and ecosystems. In most forest ecosystem studies NEE is based on eddy covariance tower measurements. Sufficient turbulence in the enclosed Biosphere 2 rainforest is lacking, invalidating the eddy covariance method (*51*). Instead, we treated Biosphere 2 as a flow-through mesocosm and measured atmospheric concentration changes within the mesocosm, as well as the flow rate and concentration of the incoming outside air. NEE was calculated for every 15-minute time step according to:

$$NEE = (CO_2^t - CO_2^{t-1}) + CO_2^{ER}$$

where the first right-hand term is the change between 15-minute time steps in moles of CO_2 inside Biosphere 2 rainforest, based on three measurement locations at different heights. CO_2^{ER} is the CO_2 adjustment due to the exchange rate. The moles of CO_2 in the rainforest were calculated according to:

$$CO_2 = \sum \frac{V_{TRF} * F_{Zone} * P}{(273.15 + T_{Ave}) * R} * \frac{[CO_2]}{10^6}$$

where V_{TRF} is the rainforest volume (27,700 m^3; (*19*)), F_{Zone} is the volume fraction of the height zone based on geometric calculations (0.304, 0.588, and 0.108, for Zone C1, C2, and C3 respectively), P is the air pressure, R the gas constant and $[CO_2]$ the CO_2 concentration.

The exchange rate (ER) CO_2 adjustment was calculated based on:

$$CO_2^{ER} = \left(\frac{[CO_2^{27m}]}{10^6} - \frac{[CO_2^{Out}]}{10^6}\right) * \frac{V_{TRF} * ER * P}{(273.15 + T_{27m}) * R}$$

The outside air was measured once an hour in the inflow tube with a dual laser QCL (Aerodyne, Billerca, MA, USA). Gaps in the QCL record were filled with CO_2 data from two nearby locations: 1) a well-ventilated space without plants in the Biosphere 2 (Landscape Evolution Observatory (*52*)) and 2) the Santa Rita Experimental Range NEON site.

From the NEE, we calculated ecosystem respiration (R_{eco}) by taking the mean nighttime NEE per day, according to (*21*). Then gross primary production (GPP) was calculated from: GPP = NEE + R_{eco} and daily values were reported based on the sum of the GPP values.

Evapotranspiration

Whole ecosystem evapotranspiration (ET, the loss of water (H_2O) from ecosystems to the atmosphere) was calculated based on the water balance from each 15-minute time step according to:

$$ET = \frac{\Delta H_2O + (H_2O_{27m} - H_2O_{out}) * ER * V_{TRF} + \Delta H_2O_{AHU} + \Delta H_2O_{Dehumid} + \Delta H_2O_{Glass}}{Area}$$

where the first right-hand term is the change between 15-minute time steps in kg of H_2O inside Biosphere 2 rainforest, based on 18 measurement locations at different heights. H_2O_{27M}, H_2O_{Out}, H_2O_{AHU}, $H_2O_{Dehumid}$, and H_2O_{Glass}, are the kg of H_2O at the top of the rainforest, where the main air outflow louvers are, H_2O in outside air, H_2O removed during cooling with the AHU, H_2O removed when one AHU was used to dehumidify (first cool and then heat the air) the rainforest for the enhanced drought phase, and the maximum amount of water removed by condensation on the glass when the outside air temperature was much lower than the inside temperature. Hourly ET was divided by four for the 15-minute time steps. Area and V_{TRF} denote the rainforest ground surface area and volume (1940 m^2 and 26,700 m^3; (*20*)).

The same HMP45C probes (Vaisala Oyi., Vantaa, Finland) used to calculate VPD were used to calculate the vapor density (VD, in kg m^{-3}) using the following equation (based on (*53*) and the ideal gas law):

$$VD = \frac{0.002166 * \left(610.78 * e^{\frac{T}{(T+238.2)} * 17.2694}\right) * \left(\frac{RH}{100}\right)}{(T + 273.15)}$$

where T stands for temperature and RH the relative humidity measured at each location.

All temperature data were averaged over the five height zones (Fig. S3) as determined by the sensor locations for the final calculations. The mass of H_2O (kg) in the rainforest air was calculated according to:

$$H_2O = \sum_{x=1}^{5} V_{TRF} * F_{Zone} * VD_{Zone}$$

where TRF stands for the whole rainforest and Zones X = 1 through 5 are the different height zones outlined in Fig. S3, and F_{Zone} is the volume fraction of the height zone based on geometric calculations (0.176, 0.360, 0.243, 0.135 and 0.086, for Zone 1 through 5 respectively).

Six AHUs were constantly used to control the temperature within the Biosphere 2 rainforest. During cooling phases, when the rainforest temperature was exceeding the target temperatures, the AHUs would also reduce the air water content through condensation. The amount of air removed by the AHUs during cooling was calculated based on:

$$H_2O = \sum_{x=1}^{AHU} v_{Out} * Area_{AHU} * (VD_{AHUIn} - SatVD_{AHU}) * e_{AHU}$$

where v_{Out} is the air outflow velocity (m/s) of the AHU, $Area_{AHU}$ is the outflow area of the AHU, and VD_{AHUIn} is the vapor density of the air coming into the AHUs based on the outside T, RH, and airflow (which enters the Biosphere 2 rainforest just before the AHU) and based on the remaining AHU outflow volume air and the T and RH at NW tower 1 and 3m heights (closest to the return air intake), and e_{AHU} is a water removal efficiency of the AHU based on the comparison of this method with the weather station (WeatherHawk) units placed at inflow and outflow points of different AHUs to test their efficiency.

The change in water across the dehumidifying AHU #1 for each 15-minute time step was calculated based on:

$$H_2O_{Dehumid} = v_{Out} * Area_{AHU} * (VD_{Out} - VD_{In})$$

where VD_{In} and VD_{Out} are the inflow and outflow vapor densities based on the T and RH of the WeatherHawk sensors in the inflow and outflow areas of the AHU.

During the winter months, outside air temperatures dropped well below inside air temperatures, causing the water vapor in the TRF to condense on the inside of the glass and steel space frame structure. The amount of water lost from the air through condensation on the glass space-frame (H_2O_{Glass}) was calculated based on the assumption that the average of the outside and inside air temperature represented the glass temperature. We calculated the condensation potential based on how far the saturation VD at the glass temperature was below the VD at that height zone inside the rainforest. We scaled the condensation potential in each height zone by its glass surface area to calculate H_2O_{Glass}.

Composition and Gas Exchange of Ecosystem Compartments

The B2-WALD online gas measurement system consisted of multiple instrument streams (9 total; here data were derived from instrument streams S1, S2, S3, and S5) (Fig. S9; Table S7) of integrated CO_2, H_2O, and VOC analyzers (as in (*54*)) to measure atmospheric composition and leaf, stem, and soil fluxes from 56 measurement locations in the ecosystem. The gas analyzers were housed within the TRF mountain feature, predominantly within a climate-controlled shed (~27 °C). Gas sampling was coordinated by automated valves that directed gas through the instrument streams to multi-analyzer sampling loops in the climate-controlled shed. We avoided condensation in gas lines and valves by heating the lines or placing sample selection apparatus in a warm room annexed to the shed. Zero air was centrally generated and used directly (e.g., for instrument reference) or mixed with cylinder gas to generate gas mixtures with controlled composition gas (e.g., inlet gas to leaf chambers, online calibration mixtures). The air was compressed by an in-house oil-free air compressor (Kaeser Compressors Dental, 11 CFM, model Dental 3/2T type 117 769), filtered for impurities and condensation, and purified with a zero air generator (ZAG) (Aadco Instruments, Inc., Cleves, OH. 737-13-C-CH4-120) that removed methane and volatile compounds, as well as CO_2 with add-on scrubbers (PureGas, VCD4-12-029). Wherever possible, we used teflon tubing (PFA) and fittings (PFA Swagelok, PEEK IDEX, PEEK VICI ferrules, and PFA Galtek) upstream of VOC analyzers to minimize surface VOC losses and conversions.

Calibration of CO_2 and H_2O isotope analyzers

We used a Central Calibration Unit (CCU) to provide CO_2 and H_2O in different concentrations and isotopic compositions to calibrate the laser spectrometers (LAS; Table S7) that quantify trace gas concentrations and isotope ratios by infrared absorption spectroscopy. The CCU main air flow (zero air, 1 L min^{-1} through the nebulizer and 4 L min^{-1} make-up air) was provided by the ZAG and metered through two Mass Flow Controllers (MFC; Alicat, Tucson, AZ, USA). The nightly CCU procedure covered 14 stages over an 80-minute period (0:00-1:20) that covered a range of CO_2 (0 to 1600 ppm) and H_2O (0 to 25,000 ppm) concentrations crossed with a gradient in isotopic composition (see description below). All five analyzers were switched via 3-way solenoid or multiport valves to sample the common calibration gas. The CCU was controlled by a control system (National Instruments, Austin, TX, USA), and CO_2 and H_2O concentrations were randomly selected, while each of the isotopic compositions were selected sequentially.

To generate carbon dioxide isotope calibration curves using the CCU, we added different quantities of 5% CO_2 in air (Airgas Inc., Wayne, PA, USA) through MFCs to yield four different CO_2 concentrations between 300 and 1500 ppm CO_2 in air. This was done for three different isotopic compositions using reference tanks from different geographical regions (La Porte, TX, Tooele, UT, and Phoenix, AZ) that had characteristic $\delta^{13}C$ values of CO_2 (~-10, -32.8, and -38.9‰, respectively). Tanks of the most enriched mixture (~-10‰) from Texas were replaced approximately every two weeks, as the 5 % CO_2 was also used to supply leaf mix CO_2 (see *Leaf Measurements*, below). We used LAS-2 (Table S7) and its two internal isotopic composition reference gases (-8 and -27 ‰, VPDB, Thermo Fisher, Scientific, Germany) to directly calibrate all CCU tank $\delta^{13}C$ values.

To generate water isotope calibration curves using the CCU, we metered water of three different δ^2H values (~-140.3, +25.0 and +454.6‰ vs VSMOW) into zero air using a micro peristaltic pump (Periwave Milli, CorSolutions, Ithaca, NY, USA). Water was vaporized within a glass nebulizer (High Efficiency Nebulizer, Meinhard, Golden, CO, USA). The metal nebulizer housing and the zero air stream coming into the nebulizer were heated to 150 °C and 120 °C, respectively, to prevent condensation in the chamber. Water concentrations (up to 25,000 ppm H_2O) were changed by modulating the peristaltic pump rate, while the hydrogen isotopic composition was changed by selecting different waters with a Valco multiport valve (VICI Valco Instruments, Houston, TX, USA). δ^2H values of CCU standard waters were determined from liquid samples at the Chair of Ecosystem Physiology, Freiburg using cavity ring-down spectroscopy (L2130i Water Isotope Analyzer, Picarro Inc., Santa Clara, CA, USA), using four house standards (δ^2H values = -102.8, -63.7, -10.22, and +53.9‰, VSMOW) cross-calibrated to international standards GISP, SLAP and SMOW (IAEA, Vienna).

Analyzers either directly sampled the CCU on a nightly basis or were cross-referenced to this or other primary calibrations. The S1 nightly CCU procedure was used to account for LAS-1 concentration-dependent offsets between true and observed isotope ratios using $\log_2$ and linear functions for ^{13}C and ^2H isotopes of CO_2 and H_2O, respectively, as a function of their respective bulk concentrations. LAS-1 CO_2 concentrations were cross-calibrated with LAS-2 values through simultaneous measurement of the controlled leaf gas mixture (~500 ppm CO_2) throughout the campaign by both instruments (see *Leaf Measurements* below). For S2, the two internal LAS-2 standards (described above) were diluted with CO_2-free ultra-high purity nitrogen gas (Airgas Inc., Wayne, PA, USA) to match the concentration of the sample gas and were used for continuous calibration of the $\delta^{13}C$ values measured by this analyzer. The LAS-2 internal calibration procedure included isotopic linearity calibration, two-point concentration calibration as well as a two-point δ scale calibration. The CO_2 isotope analyzers of S3 (LAS-4) and S5 (LAS-5) were calibrated to the VPDB scale using the nightly CCU procedure, accounting for span and offset. Concentration measurements of LAS-5 were verified with an external gas standard (1500 ppm ±1% CO_2 in synth. air) measured several times a day. Throughout the experiment, concentration measurements were stable and within the range of uncertainty of that external standard. Concentration measurements by LAS-4 were calibrated (span-offset) using the nightly CCU-procedure.

Calibration of proton transfer reaction time-of-flight mass spectrometry (PTR-TOF-MS) instruments

Nocturnal calibrations of all proton transfer reaction time-of-flight mass spectrometers (PTR-TOF-MS) were conducted using a liquid calibration unit (LCU, Ionicon Analytik, Austria) supplied by the ZAG and one of two standard gas cylinders containing different multi-VOC component calibration mixtures (Table S8) in Ultra-High Purity (UHP) nitrogen (Apel-Riemer Environmental, Inc., Florida, USA). The LCU delivered the controlled calibration mixture to each PTR-TOF-MS via 3-way valves (Parker Hannifin, Teflon(R), 001-0028-900, Ohio, USA) through ⅛" PFA tubing heated to 50 °C with a custom-made heating system. Each night at midnight, all the PTR-TOF-MS instruments switched to sample LCU output dynamic calibration 5-step routine for 75 minutes. In order to ensure the full standard equilibration, the gas standard was set to start flowing one hour prior to the start of calibration. The zero air flow rate was held constant (typically 1000 sccm), while the gas standard flow rate was changed every 15 min starting from 40 sccm until 0 sccm in 10 sccm steps. The liquid feed of the LCU drew Milli-Q water from a reservoir, which was dynamically nebulized into the evaporation chamber at 20 µL/min to reach a similar humidity level of the calibration mixture as observed in the B2 TRF atmosphere.

The two calibration standard cylinders (Table S8) were used during the campaign to allow explicit calibration of a wide range of species and to evaluate transmission efficiency of the broad *m/z* range. The first cylinder was used for two periods (from 18 September 2019 to 6 November 2019 and from 17 December 2019 to 20 January 2020) to account for any reduction in sensitivity or transmission of the PTR-TOF-MS instruments as a function of detector aging over the campaign. The second cylinder was used from 7 November 2019 to 16 December 2019 to complement the suite of calibrated VOCs.

The ion yields of all m/z were measured in counts per second (cps) and compounds were identified from the measured exact mass of their protonated parent ions and isotopic patterns. To account for possible variations of the

reagent ion signals, measured ion intensities were normalized to the H_3O^+ counts in combination with the water-cluster ion counts (*55*). All PTR-TOF files were processed using the software *PTRwid* (*56*). Data analysis of stream 2 was performed by PTRMS Analysis (PTRMS-analysis.com). Concentrations of compounds not included in the calibration standard cylinders were calculated applying the kinetic theory of proton transfer reaction (*57, 58*).

Atmospheric measurements

Atmospheric gas concentrations of CO_2, H_2O, and VOCs and selected isotopologues were measured hourly over five-minute intervals at five different heights (1 m, 3 m, 7 m, 13 m and 20 m) above the forest floor from the NE tower (S1) and at the outside air inlet to the ecosystem, with duplicate measurements every other hour for heights 3 m and 13 m (S2). All sampling lines had a length of 30 m and were made of ¼" OD PFA tubing (Ametek, Nesquehoning, PA, USA) that was protected by inlet filters (0.45 µm pore size PTFE; EW-02915-31, Cole Palmer, Vernon Hills, IL). Within each five-minute valve interval we averaged two minutes of data (from minute 2.5 to 4.5) after quality control filtering.

The isoprene ^{13}C isotope ratio was calculated as the ratio of $[^{13}C]C_4H_8$ concentration to C_5H_8 concentration and the monoterpene ^{13}C isotope ratio was calculated as the ratio of $[^{13}C]C_9H_{16}$ concentration to $C_{10}H_{16}$ concentration. Since both isoprene and monoterpene signals were explicitly calibrated, we assumed that the sensitivities of the ^{12}C and ^{13}C analogue of each VOC were identical. During the nighttime, concentrations of the ^{13}C analogue fell below the MS-1 detection limit, so only daytime isotope ratios are reported. The enrichment of the ^{13}C VOCs shown in Fig. 4f and 4g are the elevated isotope ratios above the background level. The background isotope ratio, with ^{13}C naturally occurring at 1.109 % of all carbon and ^{12}C naturally occurring at 98.89 % of all carbon, was calculated as 1.109/98.89 = 1.112. As isoprene contains 5 and monoterpenes contain 10 carbon atoms, the background, single-carbon isotope ratio was multiplied by 5 and 10 to find the ^{13}C isoprene and ^{13}C monoterpene isotope ratios, respectively.

Leaf measurements

Leaf fluxes were measured every hour (S1), every two hours (S2), or every 25 minutes (S7) over five-minute intervals using a total of 30 leaf and empty chambers (S1: 5 chambers, S2: 20 chambers, S7: 5 chambers) (Table S6; Table S7). Custom-built flow-through leaf-chambers were constructed out of FEP film (McMaster Carr, 85905K64, Elmhurst, IL, USA). Structure was provided by copper wire threaded through PFA tubing (⅛" OD; Ametek, PA, USA). Leaf chambers were equipped with a fan (MC25101V2, Sunon, Taiwan) to guarantee effective air mixing and were sealed with terostat (Terostat-II, Kahmann & Ellerbrock GmbH & Co. KG, Bielefeld, Germany) on both ends. We generated a controlled gas composition by metering 5 % CO_2 in air (using the $\delta^{13}C$ ~ -10 ‰ tanks from the CCU) into VOC-free ZAG air. During $^{13}CO_2$ pulse labeling, an additional low flow mass flow controller (MFC) was added to the gas mixing system (P_{pre}: Bronkhorst F-200CV-005-AAD-22-V, MFC-4 at 1.47 sccm; P_{dro}: Alicat Scientific, Inc. MC-2SCCM-D/5M re-ranged to MC-4SCCM-D/5M, MFC-50 3.21 sccm) at a rate to match the atmospheric $^{13}CO_2$ enrichment (see *Ecosystem-Scale Isotope Labeling* above). The air was humidified via selectively permeable membrane Nafion tubing, enabling the transfer of water vapor between purified water (Barnstead™ Nanopure™, Thermo Fisher Scientific, Dubuque, IA, USA) and the gas stream (MH-110-48F-4; Perma Pure, LLC, Lakewood, NJ, USA). The custom gas mixture was delivered via a distribution manifold (custom aluminum blocks with ports) to 24 MFCs (MC-2SLPM-D/5M, MCS-2SLPM-D-.25NPT/5M; Alicat Scientific, Inc., Tucson, AZ, USA) to continuously flush each of the 25 chambers with 1 L min^{-1} of VOC-free air with ~500 ppm of CO_2 and ~2000 ppm of H_2O. For less active leaves the flow was reduced to 0.85 L min^{-1} to increase the leaf signal, while for the biggest leaf (PA4) the flow was increased to 1.45 L min^{-1} to prevent water condensation in the chamber. This approach balanced leaf drying by inlet air against potential condensation of plant-released moisture in sample outlet air. Leaf temperature (°C) and PAR (µmol m^{-2} s^{-1}) were logged for each chamber. Sampling lines were heated to prevent condensation. Over each five-minute measurement interval, two-minute averages (from minute 2.5 to 4.5) of each CO_2 and H_2O isotopologue were computed.

Calculation of leaf fluxes

The isotopic composition of leaf CO_2 ($\delta^{13}C_l$; ‰, VPBD) and H_2O (δ^2H_l; ‰,VSMOW) were calculated using isotopic mass balance:

$$\delta^{13}C_l = (\delta^{13}C_0 c_0 - \delta^{13}C_e c_e)/(c_0 - c_e) \quad (1)$$

$$\delta^2H_l = (\delta^2H_0 w_0 - \delta^2H_e w_e - (\delta^2H_0 - \delta^2H_e)\, w_0 w_e)/(w_0 - w_e) \quad (2)$$

where c_e is the CO_2 concentration in the empty chamber, c_o is the CO_2 concentration at the exit of the leaf chamber, w_e is the concentration of water vapor in the empty chamber, w_0 is the concentration of water vapor at the exit of the leaf chamber, $\delta^{13}C_0$ and δ^2H_0 are the delta values of the air leaving the leaf chamber, and $\delta^{13}C_e$ and δ^2H_e are values for air measured in the empty chamber.

The mean residence time of ^{13}C-tracer in leaf respiration after each atmospheric pulse labeling was calculated from the δ^{13}C values of leaf nighttime respiration. An exponential decay model was fitted to the δ^{13}C values of leaf respiration. Mean residence time was calculated as the time required to reduce the δ^{13}C value of leaf respiration to 1/e of its initial value.

Criteria for functional group assignment

We assigned all measured canopy-forming trees and understory species into different functional groups regarding their drought susceptibility (drought-tolerant and drought-sensitive) based on their anatomical and hydraulic traits (growth form, specific leaf area, wood density) and functional response to drought (Table S1). The functional drought response was assessed for each individual plant in terms of the magnitude and velocity of changes. Thus, beyond assigning species based on their anatomical traits, we evaluated functional changes of sap flux rates, leaf water potentials, and transit times assessed from labeling with respect to their response velocity during early/late drought and rewet and response magnitude (% decrease during drought). The analysis revealed that the positioning within the forest strata with different microclimate, in particular light climate and VPD, had a significant impact on the functional response of the different plant individuals. Therefore, grouping was adjusted based on the functional response taking both the species drought adaptation and their environment/positioning within the forest into account, resulting in the four assigned functional groups of drought-tolerant and drought-sensitive canopy-forming trees and drought-tolerant and drought-sensitive understory species as shown in Table S1.

We calculated mean carbon and water fluxes of SF, δ^2H_l, pLWP, and mLWP for each functional group, as well as group contributions to the total ecosystem flux. Total water flux was normalized to the pre-drought phase (mean values from 4 October to 7 October). All later periods had lower fluxes and exhibited relative total water flux < 100%. Then, the relative contribution of each functional group to the normalized flux was derived. For SF, daily sums were calculated. δ^2H values of transpiration (δ^2H_t) were derived by averaging δ^2H_l values each day. Smoothing functions were calculated separately for the periods before and after the deep rewet (December 1 - 3, 2019) using locally estimated scatterplot smoothing (predict function, R version 3.6.0). For continuous data (SF, δ^2H_t) the transit period (December 1 - 3, 2019) was linearly interpolated. In the case of mLWP, the transit time was November 30 - December 3, 2019 (understory) and December 1 - 3, 2019 (canopy). For pLWP, no data were collected directly before rewet (December 1, 2019). Therefore, no interpolation was applied across the transition period.

Soil flux measurements

Soil fluxes of CO_2 and VOCs were measured continuously by an automated soil flux system consisting of a LI-8100 infrared gas analyzer (IRGA) and a LI-8150 16-port multiplexer (Licor Inc., Lincoln, NA, USA) and 12 closed dynamic soil flux chambers (LI 8100-104 Long-Term Chambers with opaque lids, Licor Inc.). The chambers were placed on pre-installed PVC-collars (20 cm diameter). Collars were installed in vegetation-free, bare soil several weeks before the start of the measurements. Each chamber measurement lasted for 10 minutes and consisted of 2.5 minutes of pre-purge (chamber open, lines flushed), followed by 6.5 minutes of closure time and 1 minute of post-purge. All 12 chambers were measured consecutively. Hence, each chamber was measured once every two hours. The system volume (chamber volume, tubing, multiplexer and IRGA) was between 6.5 to 7 L. To integrate additional trace gas analyzers to measure soil CO_2 fluxes (LAS-4) and soil VOC fluxes (MS-3, Table S7) into the system, a subsample of ca. 100 sccm was directed from the outflow of the LI-8100A and distributed to the different analyzers. To avoid effects of negative pressure in the system, the volume of subsampled air was replaced with an identical volume of inflow of constant air supplied from the CCU. The outflow of subsample and the inflow of make-up gas were controlled with MFCs (Alicat, Tucson, AZ, USA). The gas composition of the CCU makeup gas was measured on Stream 3 for 10 minutes after every measurement cycle.

Soil Flux Calculations

We calculated soil CO_2 efflux rates with linear and exponential models, fitted to each individual chamber measurement. We omitted the first 30 s after chamber closure to allow for mixing in the just-closed chamber. For the linear models we used the first 120 s after chamber closure, and for the exponential models the full closure time. The exponential model is formulated as

$$c(t) = c_\infty + (c_0 + c_\infty)\, e^{-\alpha(t-t_0)}$$

where c0 is the starting concentration, t is time, and t0 the time of chamber closure. The efflux is derived from dc(t)/dt at t0. In cases where the algorithm failed to fit the exponential model, flux rates derived from linear models were used.

To calculate $\delta^{13}C$ values of soil-respired CO_2 we used the Keeling plot approach with model I linear regression (*57*). The first 30 s of each observation were excluded. Quality of CO_2 fluxes and $\delta^{13}C$ values were checked visually and outliers were removed prior to further analysis. CO_2-fluxes and $\delta^{13}C$ values of CO_2 were aggregated to daily mean values for each soil chamber.

We calculated soil VOC fluxes by applying the linear regression model to the VOC concentrations obtained during the enclosed measurement period of each chamber. We omitted the first 30 s after chamber closure to allow for mixing in the just-closed chamber. The linear regression was applied to the successive 12 data points collected at 10 s intervals. The slope of the linear regression was divided by chamber area, and a time factor to convert the results to hourly units.

Stem flux measurements

Stem respiration and the $\delta^{13}C$ values of respired CO_2 were measured continuously from 12 trees (Table S6) using a custom-made automated setup coupling steady-state flow-through stem respiration chambers to a carbon isotope analyzer (LAS-5, Table S7). The chambers were built with similar material as the leaf chambers (see *Leaf measurements*, above). They covered a base area of c. 15 x 20 cm^2. For three trees with a small circumference (Table S1) the chambers enclosed the full stem of the tree. Chambers were attached at approx. 50 cm height with tension straps around the tree stem and sealed with terostat. Each chamber had a thick inlet tube (3/4'' OD) and an outlet tube (1/4'' OD). The chamber inlet tube had a length of 50 cm and was open to ambient air around the stem. The outlet tube was connected to the multiplexing unit. At each chamber an additional gas line sampled rainforest air in direct proximity to characterize the chamber inlet composition. All chambers were continuously flushed by a central flush pump to maintain steady-state conditions inside the chambers. The flow rate in each chamber was maintained at ~ 200 sccm and logged continuously. The multiplexer switched between chamber inlets and outlets and directed the sample gas to the CO_2 analyzer. Each individual measurement consisted of 240 s of outlet measurement, framed by 180 s of inlet measurements before and after. All 12 chambers were measured consecutively, resulting in a temporal resolution of approx. 2 hours. After every second measurement cycle an external gas standard was measured for 240 s on the gas analyzer.

Stem Flux Calculations

Stem CO_2 efflux and its $\delta^{13}C$ value were calculated using two-way mixing models.

$$R_{stem} = u(CO_{2\,out} - CO_{2\,in}) \,/\, SA$$

$$\delta^{13}C_{stem} = (\delta^{13}C_{out} * CO_{2\,out} - \delta^{13}C_{in} * CO_{2\,in}) \,/\, (CO_{2\,out} - CO_{2\,in})$$

CO_2 and $\delta^{13}C$ denote the average concentrations and carbon isotopic compositions of chamber inlets and outlets, u is the molar flow and SA the stem surface area of each chamber. The first 110 s of each inlet and 210 s of each outlet measurements were omitted to ensure steady-state conditions during the averaging period. Measurements of each individual chamber were visually quality-controlled for outliers. Data was aggregated to average daily flux rates and isotopic compositions prior to further analysis.

Mean residence time of $^{13}CO_2$ in stem-respired CO_2 after the two labeling pulses was calculated for each tree by fitting exponential and polynomial decay models to the $\delta^{13}C$ values of stem CO_2 efflux. Only efflux data of the signal decay (after the maximum isotopic enrichment) was used. Polynomial models were only used when the exponential function could not be fit. Mean residence time was calculated as the time required to reduce the $\delta^{13}C$ value to 1/e of its maximum value.

Data storage and sharing

Every 15 minutes, air measurements from tower sensors were stored on centralized CR1000 data loggers (Campbell Scientific, Logan, UT, USA) with AM16/32B multiplexers (Campbell Scientific, Logan, UT, USA). The tower data loggers were connected to a centralized database with NL100 communications modules (Campbell Scientific, Logan, UT, USA). Data from the centralized database is freely available through the B2 website (www.biosphere2.org/data-models/rainforest-data). Rainforest control (AHU operation, flow through, and louver) data was automatically downloaded every 15 minutes and freely available through the B2 website (https://biosphere2.org/content/rainforest-scada-data), as is outside air temperature and moisture content data (https://biosphere2.org/research/outdoor-weather-station-data).

Sap flux, soil water content, soil matric potential, and tree water content measurements were logged every 15 minutes using SDI-12 protocols on separate CR1000 data loggers. Tree and soil pit data were manually downloaded and uploaded to a central team database. For all other instruments, data was stored on the computer operating the instrument and uploaded on a weekly basis to a central Google drive.

Statistics

Leaf-level fluxes in the weeks of each pulse labeling (maximum daytime NEE and maximum nighttime respiration calculated as largest 10% and smallest 25% of measured fluxes of each tree in each week, respectively) and leaf ^{13}C content after each labeling were tested using linear mixed effect models. Drought, plant strategy (sensitive/tolerant) and canopy strata (canopy/understory) and the interactions of drought:strata and drought:strategy were tested as fixed effects, and individual trees were set as random intercept. Mean residence times of labeled ^{13}C stem respiration was tested with drought, plant strategy and their interaction as fixed effects. Mean residence of leaves were grouped across plant strategies and strata and tested for drought as fixed effect. Response variables were square-root or log-transformed where necessary to meet model assumptions and $\delta^{13}C$ values were transformed to atom fraction to allow data transformation. Statistical analysis was done in R. Linear mixed effect models were calculated using the package 'nlme'(60).

Leaf- and stem respired ^{13}C were tested for the effects of drought, plant strategy and canopy strata and the interactions of drought and plant strategy and drought and canopy strata using generalized additive models (GAM) and the R-package 'mgcv' (61). The smooth term accounted for the temporal dynamics of the response of each individual tree, with a maximum of eight knots. For all GAMs the methods were set to 'REML', smoothing basis to 'fs' and the family to 'scat'.

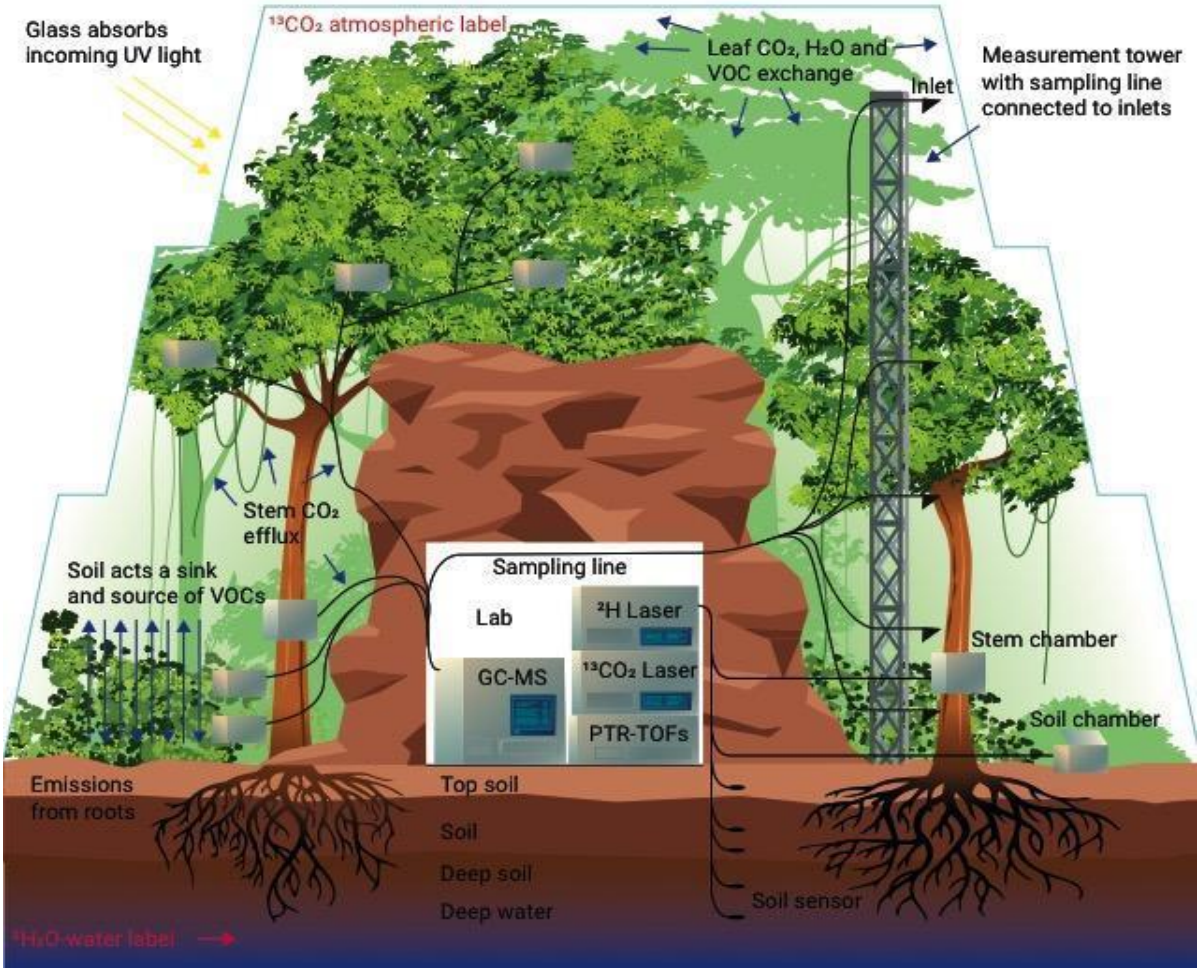

Fig. S1. Illustration of Experimental Setup in the Biosphere 2 tropical rainforest. For measuring systems and analyzers see Fig. S9

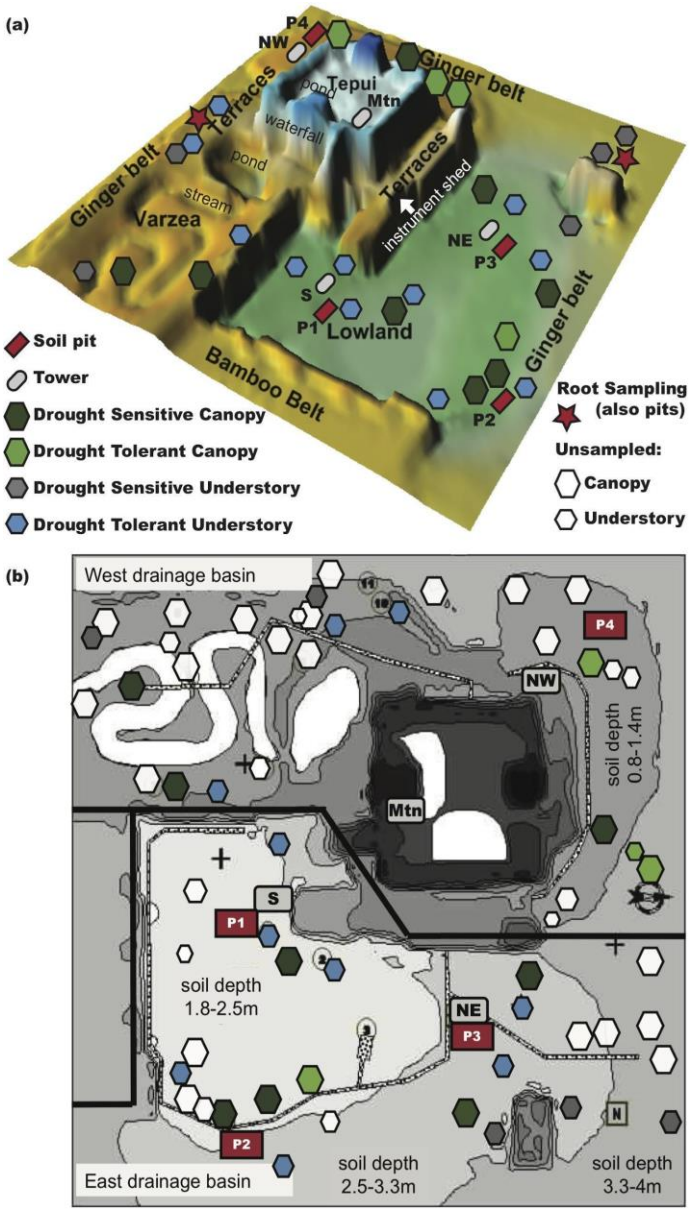

Fig. S2. Biosphere 2 tropical rainforest. (a) Topographical 3D rendering of rainforest zones and the location of water features, instrument shed, soil pits (P1 - P4), atmospheric sampling towers (NW = Northwest tower; NE = Northeast tower; Mtn = Mountain tower; S = South tower), and plants investigated. (b) Overhead 2D projection of the same features, including locations of unsampled plants (white symbols), soil depth ranges (grey shading and thin contour lines), and delineation (thick black line) between the East and West drainage basins. Soil flux chambers were installed near each of the four soil pits. Root samples were collected near each soil pit (red rectangles) and at two additional locations (red stars).

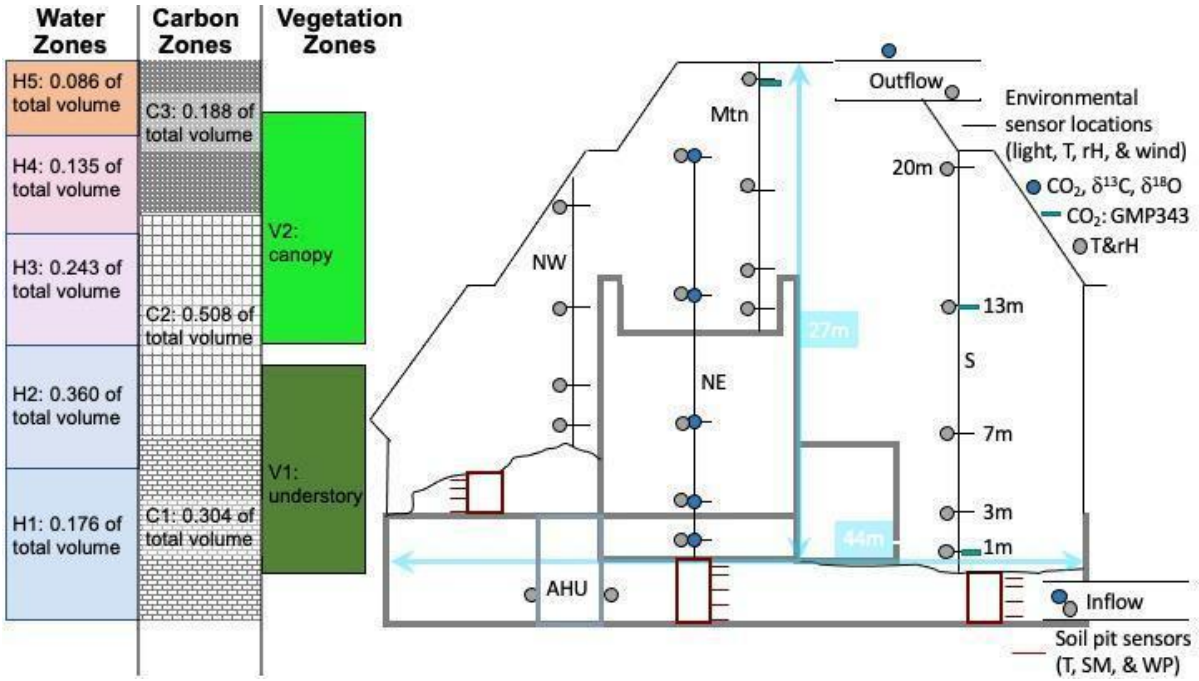

Fig. S3. Cross-section of the Biosphere 2 tropical rainforest with the environmental and CO_2 sensor locations as well as the air sampling locations for isotope and VOC measurements. At left the different color shadings indicate the height zones (H1-5) used for water budget calculations, different hatch marks indicate the height zones (C1-3) for the CO_2 budget, and the different green color shadings indicate the vegetation height zones (V1 and V2). AHU – air handler unit. Mtn – mountain tower, NE, NW, S – tower orientation in B2. T – temperature, rH –relative humidity.

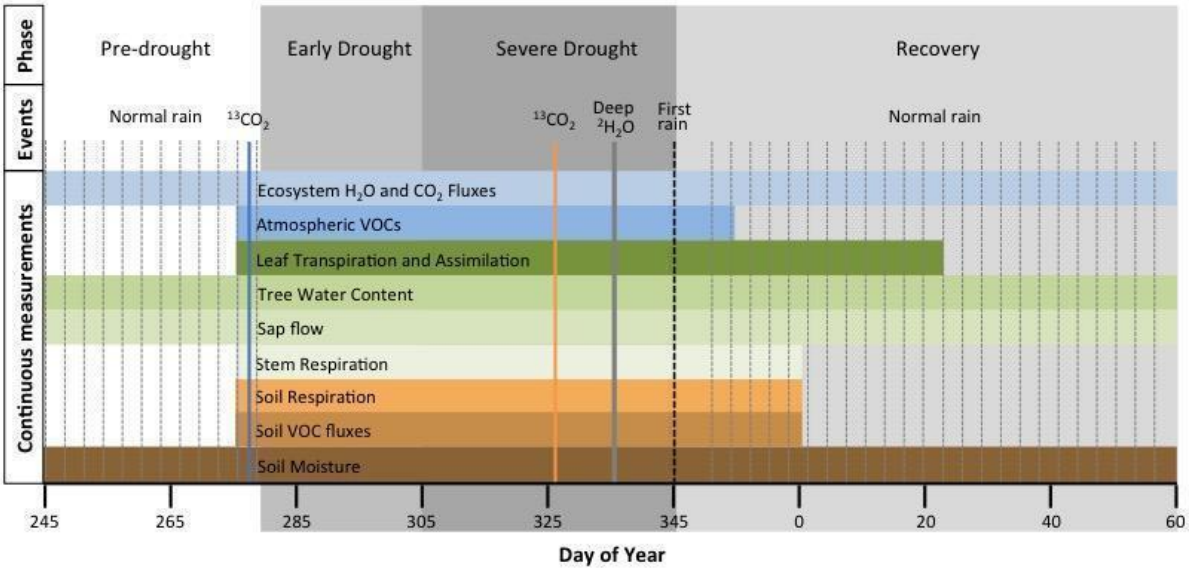

Fig. S4. Schematic overview of the experimental timeline, significant events, and continuous measurements. Regularly scheduled rain events (light dashed lines) occurred three times per week before in the pre-drought period. The early drought phase began with the first skipped rain event and lasted until the initial period of topsoil drying was complete. The severe drought phase lasted until the first rain event. We waited one week after the first rain before returning to the normal rain schedule (three events per week). We conducted ecosystem-scale $^{13}CO_2$ pulse labels in the pre-drought (solid blue line) and during the severe drought (solid orange line). We introduced ^2H_2O to the deep water late in the severe drought (solid gray line).

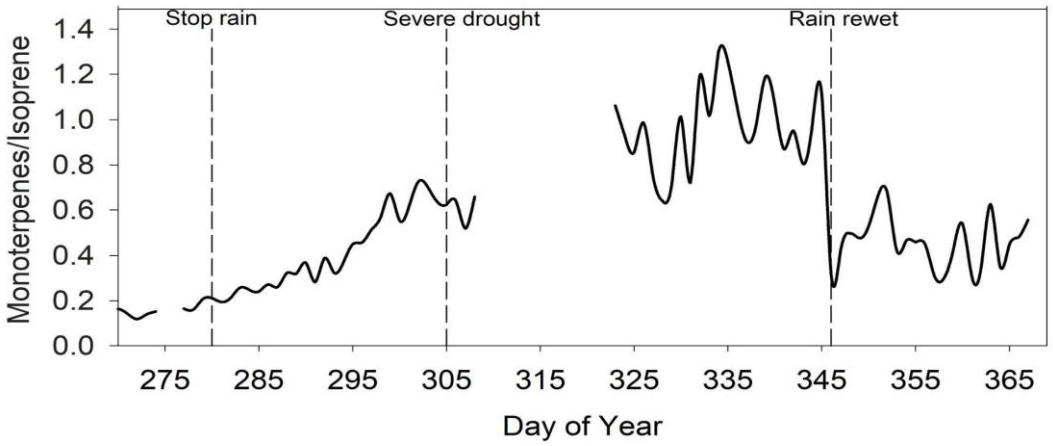

Figure S5. Soil VOC dynamics. Ratio of the soil deposition velocity (atmospheric concentration-normalized flux) of monoterpenes to that of isoprene shows an increase in the soil sink capacity for monoterpenes relative to isoprene in drought, independent of differences in real time VOC substrate availability (atmospheric concentration). This shift could reflect a greater drought sensitivity of the isoprene harvesting microbial community compared to those that use monoterpenes and/or a concordant shift in microbial VOC metabolisms with plant-controlled shifts in atmospheric availability, which is immediately reversed upon surface rewet.

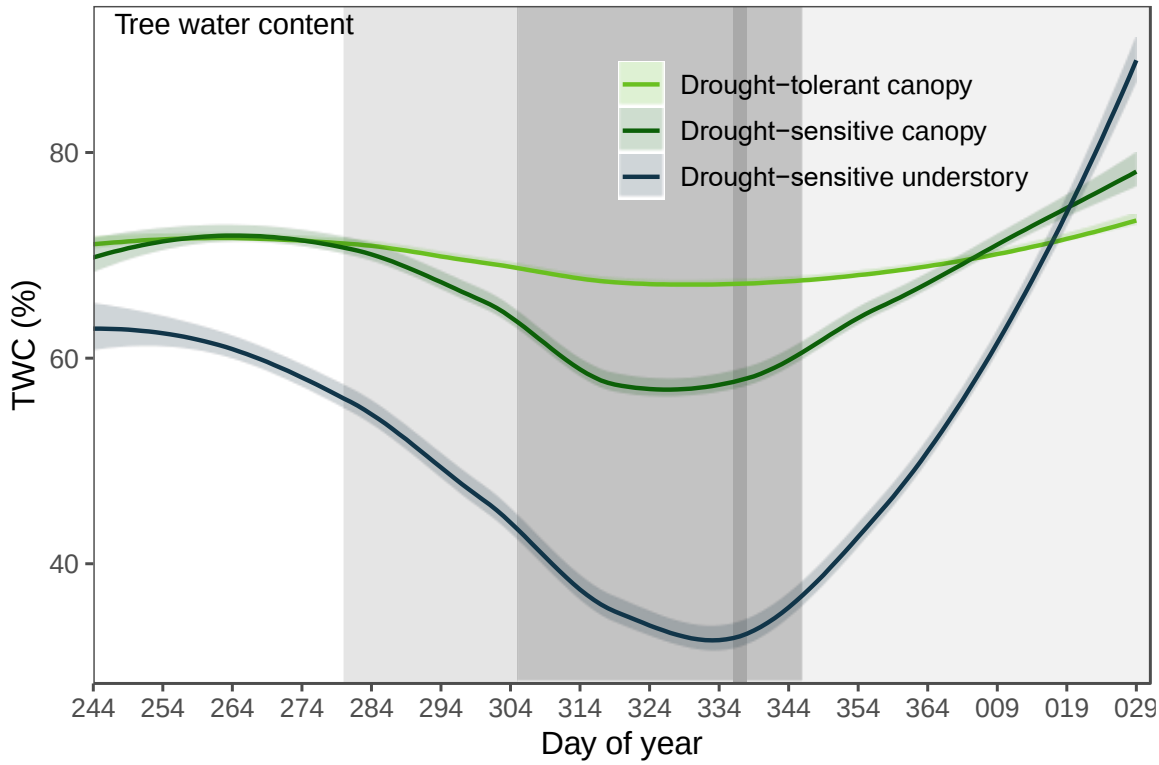

Figure S6. Tree water content (TWC, %) over time (Day of year), grouped by plant functional group (n = 2-6 per functional group). Shaded areas indicate the experiment's phases (Fig S4). Note: no data were available for TWC of drought tolerant understory. More information on data input and grouping in Supplementary Table S1 and in *Functional grouping* section of methods.

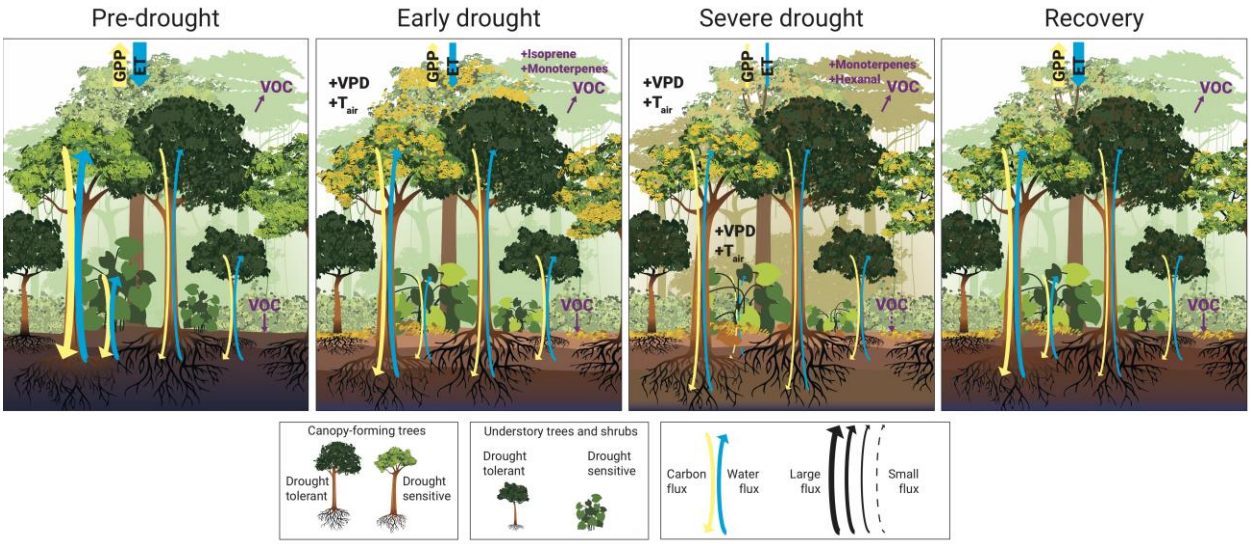

Fig. S7 Schematic ecosystem drought response indicating main processes and key drivers. Under pre-drought conditions, drought-sensitive canopy trees provide the largest contribution to total ecosystem water and carbon fluxes. Soils exhibit high net uptake of VOCs, many of which are produced in the canopy. In early drought, surface soils dry, canopy VPD increases, and plants reduce their carbon and water fluxes, with the largest reductions by drought sensitive-canopy trees. Atmospheric isoprene concentrations increase, followed by an increase in monoterpenes, while the soil becomes a more efficient monoterpene sink. In severe drought atmospheric monoterpene concentrations remain high and hexanal concentrations increase. Meanwhile, understory VPD increases to moderately high values, and the deep soil finally dries out. Ecosystem fluxes of carbon and water reach their lowest values, with the greatest individual reductions by drought-sensitive plants. Drought-tolerant plants thus become relatively more important for overall ecosystem fluxes as the drought progresses. Finally, following the reintroduction of rain, fluxes of water, carbon, and VOCs slowly recover but not to pre-drought levels for most parameters. The prolonged legacy effects of the drought are driven by slow plant hydrological recovery, reduced leaf biomass from drought-sensitive trees, and sustained reductions in soil respiration.

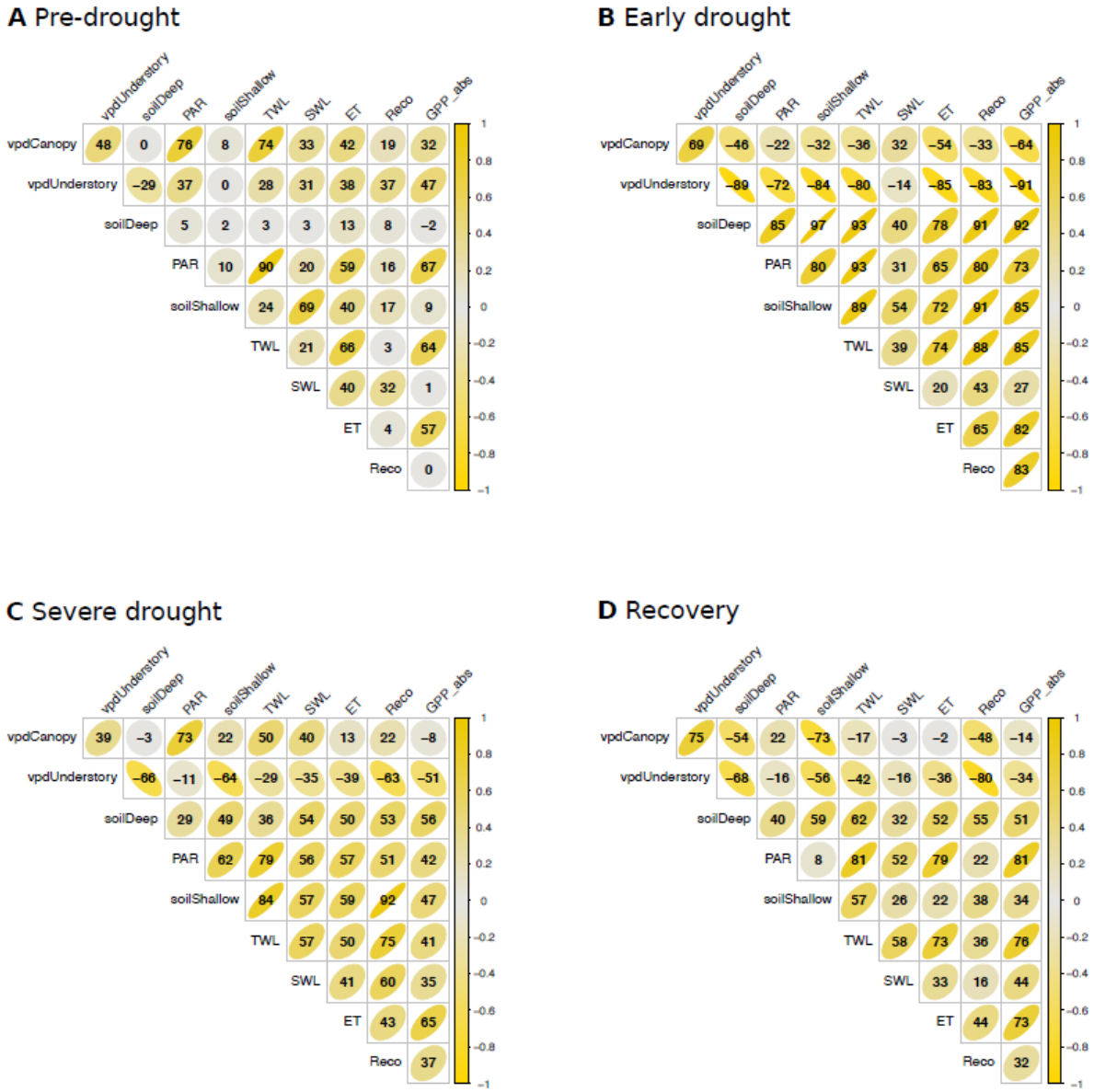

Figure S8. Correlation matrix for ecosystem fluxes and environmental drivers in each experimental phase. Colors denote strength and direction of the correlation; non-significant correlations are crossed-out (significance level < 0.05). Note that GPP is shown with a positive sign here. Correlations are based on Pearson's correlation coefficient. Abbreviations: soilDeep = matric potential in deep soil layers, soilShallow = matric potential in shallow soil layers, TWL = tree water loss, SWL = soil water loss, ET = evapotranspiration, PAR = photosynthetic active radiation, Reco = ecosystem respiration, GPP_abs = gross primary productivity (positive sign), vpdCanopy = vapor pressure deficit in canopy, vpdUnderstory = vapor pressure deficit in understory. See Material & Methods for details.

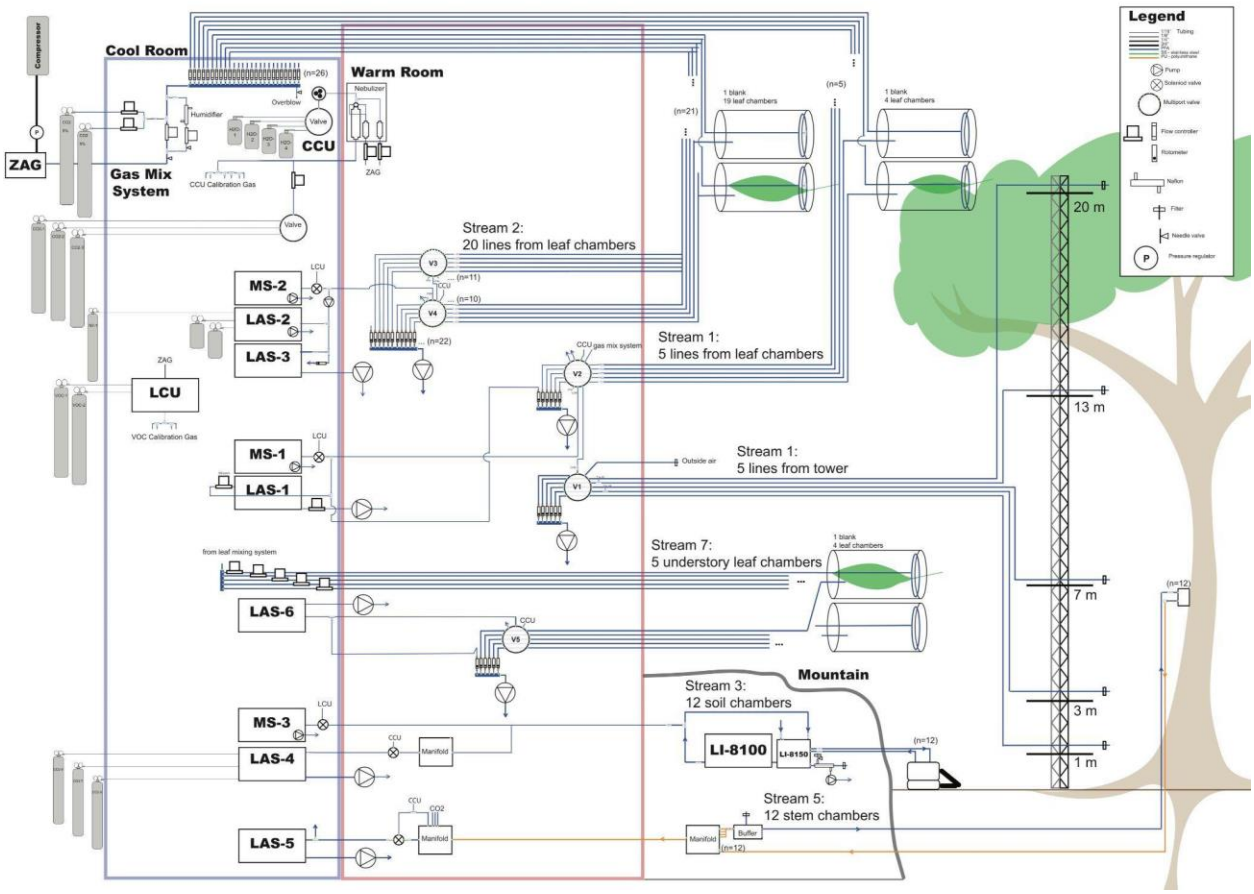

Fig. S9. Instrument system diagram illustrating the measurement streams and gas analyzers (**Table S7**) and automated gas mix systems for leaf gases and online calibration (LCU and CCU). CCU- calibration unit for CO_2, water concentration and isotopic composition, LAS – laser spectrometer; Li-8100 Licor gas analyser; LCU - liquid calibration unit for VOCs, ZAG - zero air generator.

Table S1. Plant individuals and characteristics that were used when assigning functional groups: drought-sensitive canopy (SC), drought-tolerant canopy (TC), drought-sensitive understory (SU), drought-tolerant understory (TU). DBH = diameter at breast height; LWP = leaf water potential.

Species	Plant ID	Functional group*	Wood density (g cm^{-3})	Height (m)	DBH (cm)	Light environment$^{\gamma}$	Slope of sap flow change (L d^{-2})	Slope of midday LWP change (MPa d^{-1})	Slope of predawn LWP change (MPa d^{-1})	Magnitude of midday LWP change (MPa)	Magnitude of predawn LWP change (MPa)	Maximum δ^2H value of transpired water (‰)	Days from pulse to maximum δ^2H value of transpired water
Clitoria fairchildiana	CF2	SC	0.54 ± 0.05	18	30.2	5	-0.117	-0.002	-0.006	-1	-0.65	697	13
	CF3	SC	0.53 ± 0.06	20	24.5	5	-1.285; -0.365$^{\#}$	0.001	-0.015	-0.7	-0.85	201	12
	CF4	SC	0.53 ± 0.05	25	22	4	-0.240; -0.113$^{\#}$	-0.017	-0.003	-1.03	-0.82	227	15
	CF5	SC	0.55 ± 0.03	23	25.9	4	-0.321	-0.031	-0.030	-1.13	-1.35	300	16
Ceiba pentandra	CP1	TC	0.24 ± 0.03	20	36.1	5	-0.026	0.008	0.002	-0.15		187	34
Hibiscus tiliaceus	HT1	SC	0.50 ± 0.03	25	29.3	5	-0.631	-0.017	-0.024	-1.83	-1.05	801	10
Hura crepitans	HC1	SC	0.41 ± 0.04	20	47.3	5	-0.027	-0.023	-0.022	-0.62		749	17
Pachira aquatica	PA2	TU	0.32 ± 0.04	8	12.5	2	0.001	0.008	-0.018	0.17	-0.87	-29	12
	PA3	TU	0.19 ± 0.05	6	12.5	2	-0.001					-12	13
	PA4	TC	0.37 ± 0.03	16.5	30.0	4	-0.012	-0.006	-0.007	-0.75	-0.45	145	18
	PA6	TU	0.26 ± 0.04	4		2		-0.003	-0.006				
	PA7	TU	0.29 ± 0.05	5	8.1	2						22	13
Phytolacca dioica	PD1	TC	0.17 ± 0.01	14	35.8	4	-0.016	-0.014	-0.011	-0.817	-0.53	182	34
	PD2	TC	0.17 ± 0.02	13	12	3		-0.007	-0.024	-0.95	-1.2	163	45
	PD3	TC	0.12 ± 0.02	6$^{\$}$	24.4	4		0.003	0,919	-0.32	-0.25	2	25
	PD4	TC	0.13 ± 0.01	10	22.7	5		0.018	-0.004	-0.37	-0.67		
Hibiscus rosa sinensis	HR1	TU	0.42 ± 0.01	3.7		1	-0.001	0.021	-0.012	-1.03	-0.48	-17	14
	HR2	TU	0.42 ± 0.01	3.7		1	-0.001	-0.019	-0.017	-1.08	-0.88	9	12
	HR3	SU		3.5		3	-0.013	-0.021	-0.032	-0.99	-1.46		
	HR4	SU		8.5		3		-0.016	-0.036	-2.6	-2.33		
Piper sp.	PI1	SU		4	3	3						3	46
	PI2	SU		4	3	3						66	17
	PI3	SU		4	3	3						46	41
	PI4	TU		4	3	1						22	17
Costus sp.	CO1-4	TU		~1	2	1							

* Functional group categories: drought-sensitive canopy (SC), drought-tolerant canopy (TC), drought-sensitive understory (SU), drought-tolerant understory (TU).
γ Light environment categories: always shaded = 1; mostly shaded = 2; moderately shaded = 3; slightly shaded = 4; unshaded = 5
Measurements from sap flow sensors in two stems of tree
$ Although height of PD3 < 10m, the base is located in the elevated varzia (Fig. S2) and the crown reaches the lower limits of the canopy

Table S2. Effects of campaign (pre-drought/drought), plant strategy (sensitive/tolerant), forest strata (canopy/understory) and the interactions on maximum daytime leaf-assimilation fluxes (A_{max}) and maximum leaf nighttime respiration ($Resp_{max}$)in the weeks of the labeling campaign and on bulk leaf $\delta^{13}C$ values after the labeling. F-values derived from linear mixed effect models, nominator and denominator degrees of freedom are given in subscripts. Superscripts represent respective p-values. Bold values $p < .05$, italic values $p < 0.1$

Fixed effect	Leaf A_{max}	Leaf $Resp_{max}$	Bulk Leaf $\delta^{13}C$
Campaign	**$F_{1,63}=197.17952^{<.0001}$**	**$F_{1,75}=105.11013^{<.0001}$**	**$F_{1,114}=13^{0.0005}$**
Strategy	$F_{1,11}=0.08086^{0.7814}$	$F_{1,11}=0.01166^{0.9159}$	**$F_{1,15}=6^{0.0306}$**
Strata	*$F_{1,11}=4.20975^{0.0648}$*	$F_{1,11}=1.71089^{0.2175}$	$F_{1,15}=2^{0.1749}$
Campaign:Strategy	$F_{1,63}=2.04284^{0.1579}$	$F_{1,75}=0.85557^{0.3579}$	$F_{1,114}=1^{0.2562}$
Campaign:Strata	$F_{1,63}=0.4405^{0.5093}$	$F_{1,75}=1.90155^{0.172}$	*$F_{1,114}=3^{0.0659}$*

Table S3. Effects of campaign (pre-drought/drought), plant strategy (sensitive/tolerant), forest strata (canopy/understory) and their interactions on leaf- and stem-respired $\delta^{13}C$ values in the chase periods of the two pulse labeling campaigns. Chi-square values derived from generalized additive models. Superscripts represent respective p-values. Bold values $p < .05$.

Fixed effect	Leaf-respired $\delta^{13}C$	Stem-respired $\delta^{13}C$
Campaign	$\chi^2 = 152.836^{<0.001}$	$\chi^2 = 260.624^{<0.001}$
Strategy	$\chi^2 = 0.308^{0.57898}$	$\chi^2 = 0.025^{0.873}$
Canopy	$\chi^2 = 0.69^{0.40619}$	
Campaign:Strategy	$\mathbf{\chi^2 = 10.255^{0.00136}}$	$\mathbf{\chi^2 = 16.079^{<0.001}}$
Campaign:Canopy	$\mathbf{\chi^2 = 32.926^{<0.001}}$	

Table S4. Effects of campaign (pre-drought/drought), plant strategy (sensitive/tolerant) and their interaction on the mean residence time of ^{13}C in leaf- and stem-respiration and the days between labeling and maximum $\delta^{13}C$ values in stem efflux. F-values derived from linear mixed effect models, nominator and denominator degrees of freedom are given in subscripts. Superscripts represent respective p-values. Bold values $p < .05$, italic values $p < 0.1$.

Fixed effect	MRT Leaf	MRT Stem	Max Stem
Campaign	$\mathit{F_{1,12}=3.892217^{0.072}}$	$\mathbf{F_{1,6}=12.45241^{0.0124}}$	$\mathbf{F_{1,7}=16.61777^{0.0047}}$
Strategy		$F_{1,7}=0.16691^{0.6951}$	$F_{1,7}=0.07073^{0.7979}$
Campaign:Strategy		$F_{1,6}=0.74915^{0.42}$	$F_{1,7}=0.01622^{0.9022}$

Table S5. Mean ranges of environmental conditions during the different drought phases.

	Pre-drought			Early Drought			Severe Drought			Recovery		
Zone[1]	Und	Can	Out	Und	Can	Out	Und	Can	Out	Und	Can	Out
T_{day} [°C][2]	26.6 | 21.3	35.0 | 23.3	33.5 | 21.8	29.8 | 21.8	36.6 | 23.5	27.3 | 16.5	29.6 | 22.2	34.8 | 22.6	23.6 | 5.2	28.4 | 22.8	32.5 | 23.9	19.5 | 7.6
T_{night} [°C][3]	25.1 | 20.0	26.1 | 20.9	28 | 18.0	26.6 | 20.9	26.8 | 21.5	21.4 | 12.6	25.5 | 21.2	26.0 | 21.1	17.3 | 2.6	24.4 | 21.7	25.2 | 22.4	14.3 | 4.6
VPD_{max} [kPa][4]	0.49 | 0.25	2.01 | 0.90	4.34 | 2.2	1.43 | 0.29	3.21 | 1.59	3.30 | 1.98	2.25 | 0.73	2.49 | 1.13	2.62 | 0.36	1.82 | 0.51	1.71 | 0.74	2.00 | 0.60
PAR [µmol $m^{-2}s^{-1}$][5]	135	1033	1685	75	673	1479	52	395	1016	59	474	1274

[1]Understory (Und) heights are equivalent to water Zones 1 and 2 in Figure S3; canopy (Can) equivalent to Zones 3 and 4; Out are the outside values.

[2]Day-time temperature 10th (bottom) and 90th (top) percentile quantiles. Day-time hours are when outside PAR is greater than 10 µmoles m^{-2} s^{-1}.

[3]Night-time temperature 10th and 90th percentile quantiles. Night-time hours are when outside PAR is lower than 10 µmoles m^{-2} s^{-1}.

[4]Maximum vapor pressure deficit (VPD) 10th and 90th percentile quantiles were based on the mean between 13:00 and 15:30.

[5]Maximum photosynthetically active radiation (PAR) was based on the mean between 11:00 and 14:30.

Table S6. Plant analyses. Leaf chambers were located on instrument stream 1 (S1), stream 2 (S2), or stream 7 (S7). Functional grouping of individual plants is listed in Table S1. For CF 3 and 4, two sap flow sensors were installed per tree (CF3a,b and CF4a,b).

Species	Plant ID	Leaf chambers	Bulk leaf $\delta^{13}C$ values	Leaf water potential	Stem respiration	Sap flow	Stem water content
Clitoria fairchildiana	CF2	S1	*	*	*	*	*
	CF3a	S2	*	*	*	*	*
	CF3b					*	*
	CF4a	S2	*	*	*	*	
	CF4b					*	
	CF5	S2	*	*	*	*	*
Ceiba pentandra	CP1	S2	*	*	*	*	*
Hibiscus tiliaceus	HT1	S2	*	*	*	*	*
Hura crepitans	HC1	S2	*	*	*	*	*
Pachira aquatica	PA2	S1	*	*	*	*	*
	PA3	S2			*	*	*
	PA4	S2	*	*	*	*	*
	PA6		*	*			
	PA7	S2					
Phytolacca dioica	PD1	S2	*	*	*	*	*
	PD2	S2	*	*			
	PD3	S1	*	*			
	PD4	S2	*	*			
Hibiscus rosa sinensis	HR1	S2	*	*		*	
	HR2	S2	*	*		*	
	HR3	S2	*	*		*	
	HR4	S1	*	*			
Piper sp.	PI1	S2	*	*			
	PI2	S2	*	*			
	PI3	S2	*	*			
	PI4	S2		*			
Costus sp.	CO1-4	S7					

Table S7. Instruments streams and analyzers on each stream.

Stream	Analytes	Analyzer type-No.	Model	Manufacturer	Specifications	Ecosystem compartment	Calibration
S1	H_2O, HDO, $H_2{}^{18}O$, CO_2, $^{13}CO_2$, $CO^{18}O$	LAS-1 [5]	TILDAS[1] dual CO_2 H_2O isotope analyzer	Aerodyne Research Inc., Billerica, MA, USA		Atmosphere (5 heights, TRF inlet), leaf fluxes (4 individuals & 1 blank)	CCU, LAS-2
S1	BVOCs	MS-1	PTR-QiToF-MS[2]	Ionicon Analytik GmbH, Austria	drift tube P: 3.8 mbar; drift tube T: 80 °C drift tube U: 847 V inlet T: 80 °C dwell time: E/N: 120Td		LCU
S2	CO_2, $^{13}CO_2$, $CO^{18}O$	LAS-2	Delta Ray IRIS[3]	Thermo Fisher Scientific, Bremen	with Universal Reference Interface	Atmosphere (2 heights), leaf fluxes (19 individuals & 1 empty chamber)	Internal
S2	H_2O, HDO, $H_2{}^{18}O$	LAS-3	L2120i	Picarro Inc., Santa Clara, CA, USA			Intercomparison with LAS-1; laboratory calibration for concentration dependency
S2	BVOCs	MS-2	PTR-TOF-MS 4000 ultra	Ionicon Analytik, Austria	drift tube pressure: 2.7mbar; E/N 108Td		LCU
S3	CO_2, $^{13}CO_2$, $CO^{18}O$	LAS-4	G2201i	Picarro Inc.	Interfaced with LI-8100 and LI-8150 16-port multiplexer	Soil fluxes, 12 chambers	CCU
S3	BVOCs	MS-3	PTR-TOF-MS[4] 8000	Ionicon Analytik GmbH, Austria	drift tube P: 2.2 mbar; drift tube T: 60 °C drift tube U:600 V inlet T: 60 °C dwell time:10 s E/N: 137 Td	Soil VOC fluxes, 12 chambers	LCU
S5	CO_2, $^{13}CO_2$	LAS-5	G2131i	Picarro Inc.		Stem fluxes, 12 trees	CCU, internal
S7	H_2O, HDO, $H_2{}^{18}O$	LAS-6	L2130-i	Picarro Inc.		Leaf fluxes (4 individuals & 1 empty chamber)	CCU

[1]Tunable Infrared Laser Direct Absorption Spectroscopy
[2]Proton Transfer Reaction Quadrupole Ion guide Time Of Flight Mass Spectrometer
[3]Isotope Ratio Infrared Spectrometer
[4]Proton Transfer Reaction Time Of Flight Mass Spectrometer
[5]LAS: Laser Absorption Spectrometer
MS: Mass Spectrometer, here referring to PTR-TOF-MS moieties

Table S8. VOC gas standard for daily explicit calibration and transmission calculation

Compound	Chemical Formula	Concentration Cylinder 1 [ppbV]	Concentration Cylinder 2 [ppbV]
Methanol	CH_3OH	494	433
Acetonitrile	C_2H_3N	487	461
Ethanol	C_2H_5OH	504	0
Propanal	C_3H_6O	0	463
Acetone	C_3H_6O	497	0
Isoprene	C_5H_8	509	0
DMS	C_2H_6S	537	0
Methacrolein	C_4H_6O	252	0
Methyl Vinyl Ketone	C_4H_6O	243	0
Benzene	C_6H_6	510	497
Toluene	C_7H_8	489	0
Furfural	$C_5H_4O_2$	479	0
Hexanal	$C_6H_{12}O$	0	494
Styrene	C_8H_8	0	498
m-Xylene	C_8H_{10}	0	499
Acetophenone	C_8H_8O	0	496
p-Isopropyltoluene	$C_{10}H_{14}$	0	474
α-Pinene	$C_{10}H_{16}$	0	126
β-Pinene	$C_{10}H_{16}$	0	125
3-Carene	$C_{10}H_{16}$	0	143
Limonene	$C_{10}H_{16}$	0	148
Linalool	$C_{10}H_{18}O$	466	0
α-Cedrene	$C_{15}H_{24}$	105	189
Hexamethylcyclotrisiloxane (D3)	$C_6H_{18}O_3$	502	509
Octamethylcyclotetrasiloxane (D4)	$C_8H_{24}O_4$	502	499
Decamethylcyclopentasiloxane (D5)	$C_{10}H_{30}O_5$	518	498
Dodecamethylcyclohexasiloxane (D6)	$C_{12}H_{36}O_6$	190	0

References and notes

1. G. B. Bonan, Forests and climate change: Forcings, feedbacks, and the climate benefits of forests. *Science* **320**, 1444–1449 (2008). doi:10.1126/science.1155121 Medline

2. M. Reichstein, M. Bahn, P. Ciais, D. Frank, M. D. Mahecha, S. I. Seneviratne, J. Zscheischler, C. Beer, N. Buchmann, D. C. Frank, D. Papale, A. Rammig, P. Smith, K. Thonicke, M. van der Velde, S. Vicca, A. Walz, M. Wattenbach, Climate extremes and the carbon cycle. *Nature* **500**, 287–295 (2013). doi:10.1038/nature12350 Medline

3. A. Bastos, P. Ciais, P. Friedlingstein, S. Sitch, J. Pongratz, L. Fan, J. P. Wigneron, U. Weber, M. Reichstein, Z. Fu, P. Anthoni, A. Arneth, V. Haverd, A. K. Jain, E. Joetzjer, J. Knauer, S. Lienert, T. Loughran, P. C. McGuire, H. Tian, N. Viovy, S. Zaehle, Direct and seasonal legacy effects of the 2018 heat wave and drought on European ecosystem productivity. *Sci. Adv.* **6**, eaba2724 (2020). doi:10.1126/sciadv.aba2724 Medline

4. Y. Pan, R. A. Birdsey, J. Fang, R. Houghton, P. E. Kauppi, W. A. Kurz, O. L. Phillips, A. Shvidenko, S. L. Lewis, J. G. Canadell, P. Ciais, R. B. Jackson, S. W. Pacala, A. D. McGuire, S. Piao, A. Rautiainen, S. Sitch, D. Hayes, A large and persistent carbon sink in the world's forests. *Science* **333**, 988–993 (2011). doi:10.1126/science.1201609 Medline

5. J.-P. Wigneron, L. Fan, P. Ciais, A. Bastos, M. Brandt, J. Chave, S. Saatchi, A. Baccini, R. Fensholt, Tropical forests did not recover from the strong 2015-2016 El Niño event. *Sci. Adv.* **6**, eaay4603 (2020). doi:10.1126/sciadv.aay4603 Medline

6. W. Hubau, S. L. Lewis, O. L. Phillips, K. Affum-Baffoe, H. Beeckman, A. Cuní-Sanchez, A. K. Daniels, C. E. N. Ewango, S. Fauset, J. M. Mukinzi, D. Sheil, B. Sonké, M. J. P. Sullivan, T. C. H. Sunderland, H. Taedoumg, S. C. Thomas, L. J. T. White, K. A. Abernethy, S. Adu-Bredu, C. A. Amani, T. R. Baker, L. F. Banin, F. Baya, S. K. Begne, A. C. Bennett, F. Benedet, R. Bitariho, Y. E. Bocko, P. Boeckx, P. Boundja, R. J. W. Brienen, T. Brncic, E. Chezeaux, G. B. Chuyong, C. J. Clark, M. Collins, J. A. Comiskey, D. A. Coomes, G. C. Dargie, T. de Haulleville, M. N. D. Kamdem, J.-L. Doucet, A. Esquivel-Muelbert, T. R. Feldpausch, A. Fofanah, E. G. Foli, M. Gilpin, E. Gloor, C. Gonmadje, S. Gourlet-Fleury, J. S. Hall, A. C. Hamilton, D. J. Harris, T. B. Hart, M. B. N. Hockemba, A. Hladik, S. A. Ifo, K. J. Jeffery, T. Jucker, E. K. Yakusu, E. Kearsley, D. Kenfack, A. Koch, M. E. Leal, A. Levesley, J. A. Lindsell, J. Lisingo, G. Lopez-Gonzalez, J. C. Lovett, J.-R. Makana, Y. Malhi, A. R. Marshall, J. Martin, E. H. Martin, F. M. Mbayu, V. P. Medjibe, V. Mihindou, E. T. A. Mitchard, S. Moore, P. K. T. Munishi, N. N. Bengone, L. Ojo, F. E. Ondo, K. S.-H. Peh, G. C. Pickavance, A. D. Poulsen, J. R. Poulsen, L. Qie, J. Reitsma, F. Rovero, M. D. Swaine, J. Talbot, J. Taplin, D. M. Taylor, D. W. Thomas, B. Toirambe, J. T. Mukendi, D. Tuagben, P. M. Umunay, G. M. F. van der Heijden, H. Verbeeck, J. Vleminckx, S. Willcock, H. Wöll, J. T. Woods, L. Zemagho, Asynchronous carbon sink saturation in African and Amazonian tropical forests. *Nature* **579**, 80–87 (2020). doi:10.1038/s41586-020-2035-0 Medline

7. A. B. Guenther, X. Jiang, C. L. Heald, T. Sakulyanontvittaya, T. Duhl, L. K. Emmons, X. Wang, The Model of Emissions of Gases and Aerosols from Nature version 2.1 (MEGAN2.1): An extended and updated framework for modeling biogenic emissions. *Geosci. Model Dev.* **5**, 1471–1492 (2012). doi:10.5194/gmd-5-1471-2012

8. F. Loreto, J.-P. Schnitzler, Abiotic stresses and induced BVOCs. *Trends Plant Sci.* **15**, 154–166 (2010). doi:10.1016/j.tplants.2009.12.006 Medline

9. A. Arneth, S. P. Harrison, S. Zaehle, K. Tsigaridis, S. Menon, P. J. Bartlein, J. Feichter, A. Korhola, M. Kulmala, D. O'Donnell, G. Schurgers, S. Sorvari, T. Vesala, Terrestrial biogeochemical feedbacks in the climate system. *Nat. Geosci.* **3**, 525–532 (2010). doi:10.1038/ngeo905

10. N. Unger, On the role of plant volatiles in anthropogenic global climate change. *Geophys. Res. Lett.* **41**, 8563–8569 (2014). doi:10.1002/2014GL061616

11. H. Chu, D. D. Baldocchi, R. John, S. Wolf, M. Reichstein, Fluxes all of the time? A primer on the temporal representativeness of FLUXNET. *J. Geophys. Res. Biogeosci.* **122**, 289–307 (2017). doi:10.1002/2016JG003576

12. W. R. L. Anderegg, A. G. Konings, A. T. Trugman, K. Yu, D. R. Bowling, R. Gabbitas, D. S. Karp, S. Pacala, J. S. Sperry, B. N. Sulman, N. Zenes, Hydraulic diversity of forests regulates ecosystem resilience during drought. *Nature* **561**, 538–541 (2018). doi:10.1038/s41586-018-0539-7 Medline

13. T. J. Brodribb, J. Powers, H. Cochard, B. Choat, Hanging by a thread? Forests and drought. *Science* **368**, 261–266 (2020). doi:10.1126/science.aat7631 Medline

14. H. Hartmann, M. Bahn, M. Carbone, A. D. Richardson, Plant carbon allocation in a changing world - challenges and progress: introduction to a Virtual Issue on carbon allocation: Introduction to a virtual issue on carbon allocation. *New Phytol.* **227**, 981–988 (2020). doi:10.1111/nph.16757 Medline

15. J. K. Holopainen, J. Gershenzon, Multiple stress factors and the emission of plant VOCs. *Trends Plant Sci.* **15**, 176–184 (2010). doi:10.1016/j.tplants.2010.01.006 Medline

16. N. M. Levine, K. Zhang, M. Longo, A. Baccini, O. L. Phillips, S. L. Lewis, E. Alvarez-Dávila, A. C. Segalin de Andrade, R. J. W. Brienen, T. L. Erwin, T. R. Feldpausch, A. L. Monteagudo Mendoza, P. Nuñez Vargas, A. Prieto, J. E. Silva-Espejo, Y. Malhi, P. R. Moorcroft, Ecosystem heterogeneity determines the ecological resilience of the Amazon to climate change. *Proc. Natl. Acad. Sci. U.S.A.* **113**, 793–797 (2016). doi:10.1073/pnas.1511344112 Medline

17. J. Joseph, D. Gao, B. Backes, C. Bloch, I. Brunner, G. Gleixner, M. Haeni, H. Hartmann, G. Hoch, C. Hug, A. Kahmen, M. M. Lehmann, M.-H. Li, J. Luster, M. Peter, C. Poll, A. Rigling, K. A. Rissanen, N. K. Ruehr, M. Saurer, M. Schaub, L. Schönbeck, B. Stern, F. M. Thomas, R. A. Werner, W. Werner, T. Wohlgemuth, F. Hagedorn, A. Gessler, Rhizosphere activity in an old-growth forest reacts rapidly to changes in soil moisture and shapes whole-tree carbon allocation. *Proc. Natl. Acad. Sci. U.S.A.* **117**, 24885–24892 (2020). doi:10.1073/pnas.2014084117 Medline

18. F. I. Pugnaire, J. A. Morillo, J. Peñuelas, P. B. Reich, R. D. Bardgett, A. Gaxiola, D. A. Wardle, W. H. van der putten, Climate change effects on plant-soil feedbacks and consequences for biodiversity and functioning of terrestrial ecosystems. *Sci. Adv.* 5, eaaz1834 (2019). doi:10.1126/sciadv.aaz1834

19. See supplementary materials for ecosystem fluxes during drought and recovery in an experimental forest.

20. U. Rascher, E. G. Bobich, G. H. Lin, A. Walter, T. Morris, M. Naumann, C. J. Nichol, D. Pierce, K. Bil, V. Kudeyarov, J. A. Berry, Functional diversity of photosynthesis during drought in a model tropical rainforest - the contributions of leaf area, photosynthetic electron transport and stomatal conductance to reduction in net ecosystem carbon exchange. *Plant Cell Environ.* **27**, 1239–1256 (2004). doi:10.1111/j.1365-3040.2004.01231.x

21. M. N. Smith, T. C. Taylor, J. van Haren, R. Rosolem, N. Restrepo-Coupe, J. Adams, J. Wu, R. C. de Oliveira, R. da Silva, A. C. de Araujo, P. B. de Camargo, T. E. Huxman, S. R. Saleska, Empirical evidence for resilience of tropical forest photosynthesis in a warmer world. *Nat. Plants* **6**, 1225–1230 (2020). doi:10.1038/s41477-020-00780-2 Medline

22. R. K. Monson, S. M. Weraduwage, M. Rosenkranz, J.-P. Schnitzler, T. D. Sharkey, Leaf isoprene emission as a trait that mediates the growth-defense tradeoff in the face of climate stress. *Oecologia* **197**, 885–902 (2021). doi:10.1007/s00442-020-04813-7 Medline

23. C. Werner, L. Fasbender, K. M. Romek, A. M. Yáñez-Serrano, J. Kreuzwieser, Heat Waves Change Plant Carbon Allocation Among Primary and Secondary Metabolism Altering CO_2 Assimilation, Respiration, and VOC Emissions. *Front. Plant Sci.* **11**, 1242 (2020). doi:10.3389/fpls.2020.01242 Medline

24. K. J. Jardine, J. Q. Chambers, J. Holm, A. B. Jardine, C. G. Fontes, R. F. Zorzanelli, K. T. Meyers, V. F. de Souza, S. Garcia, B. O. Gimenez, L. R. Piva, N. Higuchi, P. Artaxo, S. Martin, A. O. Manzi, Green Leaf Volatile Emissions during High Temperature and Drought Stress in a Central Amazon Rainforest. *Plants* **4**, 678–690 (2015). doi:10.3390/plants4030678 Medline

25. J. Aguirre-Gutiérrez, I. Oliveras, S. Rifai, S. Fauset, S. Adu-Bredu, K. Affum-Baffoe, T. R. Baker, T. R. Feldpausch, A. Gvozdevaite, W. Hubau, N. J. B. Kraft, S. L. Lewis, S. Moore, Ü. Niinemets, T. Peprah, O. L. Phillips, K. Ziemińska, B. Enquist, Y. Malhi, Drier tropical forests are susceptible to functional changes in response to a long-term drought. *Ecol. Lett.* **22**, 855–865 (2019). doi:10.1111/ele.13243 Medline

26. F. Zellweger, P. De Frenne, J. Lenoir, P. Vangansbeke, K. Verheyen, M. Bernhardt-Römermann, L. Baeten, R. Hédl, I. Berki, J. Brunet, H. Van Calster, M. Chudomelová, G. Decocq, T. Dirnböck, T. Durak, T. Heinken, B. Jaroszewicz, M. Kopecký, F. Máliš, M. Macek, M. Malicki, T. Naaf, T. A. Nagel, A. Ortmann-Ajkai, P. Petřík, R. Pielech, K. Reczyńska, W. Schmidt, T. Standovár, K. Świerkosz, B. Teleki, O. Vild, M. Wulf, D. Coomes, Forest microclimate dynamics drive plant responses to warming. *Science* **368**, 772–775 (2020). doi:10.1126/science.aba6880 Medline

27. D. Epron, M. Bahn, D. Derrien, F. A. Lattanzi, J. Pumpanen, A. Gessler, P. Högberg, P. Maillard, M. Dannoura, D. Gérant, N. Buchmann, Pulse-labelling trees to study carbon allocation dynamics: A review of methods, current knowledge and future prospects. *Tree Physiol.* **32**, 776–798 (2012). doi:10.1093/treephys/tps057 Medline

28. N. K. Ruehr, C. A. Offermann, A. Gessler, J. B. Winkler, J. P. Ferrio, N. Buchmann, R. L. Barnard, Drought effects on allocation of recent carbon: From beech leaves to soil CO_2 efflux. *New Phytol.* **184**, 950–961 (2009). doi:10.1111/j.1469-8137.2009.03044.x Medline

29. J. Aguirre-Gutiérrez, Y. Malhi, S. L. Lewis, S. Fauset, S. Adu-Bredu, K. Affum-Baffoe, T. R. Baker, A. Gvozdevaite, W. Hubau, S. Moore, T. Peprah, K. Ziemińska, O. L. Phillips, I. Oliveras, Long-term droughts may drive drier tropical forests towards increased functional, taxonomic and phylogenetic homogeneity. *Nat. Commun.* **11**, 3346 (2020). doi:10.1038/s41467-020-16973-4 Medline

30. S. Haberstroh, M. C. Caldeira, R. Lobo-do-Vale, J. I. Martins, J. Moemken, J. G. Pinto, C. Werner, Nonlinear plant-plant interactions modulate impact of extreme drought and recovery on a Mediterranean ecosystem. *New Phytol.* **231**, 1784–1797 (2021). doi:10.1111/nph.17522 Medline

31. W. R. L. Anderegg, A. T. Trugman, D. R. Bowling, G. Salvucci, S. E. Tuttle, Plant functional traits and climate influence drought intensification and land-atmosphere feedbacks. *Proc. Natl. Acad. Sci. U.S.A.* **116**, 14071–14076 (2019). doi:10.1073/pnas.1904747116 Medline

32. M. Dubbert, C. Werner, Water fluxes mediated by vegetation: Emerging isotopic insights at the soil and atmosphere interfaces. *New Phytol.* **221**, 1754–1763 (2019). doi:10.1111/nph.15547 Medline

33. M. Sprenger, C. Stumpp, M. Weiler, W. Aeschbach, S. T. Allen, P. Benettin, M. Dubbert, A. Hartmann, M. Hrachowitz, J. W. Kirchner, J. J. McDonnell, N. Orlowski, D. Penna, S. Pfahl, M. Rinderer, N. Rodriguez, M. Schmidt, C. Werner, The Demographics of Water: A Review of Water Ages in the Critical Zone. *Rev. Geophys.* **57**, 800–834 (2019). doi:10.1029/2018RG000633

34. E. Y. Pfannerstill, A. C. Nölscher, A. M. Yáñez-Serrano, E. Bourtsoukidis, S. Keßel, R. H. H. Janssen, A. Tsokankunku, S. Wolff, M. Sörgel, M. O. Sá, A. Araújo, D. Walter, J. Lavrič, C. Q. Dias-Júnior, J. Kesselmeier, J. Williams, Total OH Reactivity Changes Over the Amazon Rainforest During an El Niño Event. *Front. For. Glob. Change* **1**, 12 (2018). doi:10.3389/ffgc.2018.00012

35. U. Pöschl, S. T. Martin, B. Sinha, Q. Chen, S. S. Gunthe, J. A. Huffman, S. Borrmann, D. K. Farmer, R. M. Garland, G. Helas, J. L. Jimenez, S. M. King, A. Manzi, E. Mikhailov, T. Pauliquevis, M. D. Petters, A. J. Prenni, P. Roldin, D. Rose, J. Schneider, H. Su, S. R. Zorn, P. Artaxo, M. O. Andreae, Rainforest aerosols as biogenic nuclei of clouds and precipitation in the Amazon. *Science* **329**, 1513–1516 (2010). doi:10.1126/science.1191056 Medline

36. L. Meredith *et al*., B2WALD campaign team and contributions, Version 2, University of Arizona Research Data Repository (2021). doi:10.25422/azu.data.14632662

37. T. C. Taylor, S. M. McMahon, M. N. Smith, B. Boyle, C. Violle, J. van Haren, I. Simova, P. Meir, L. V. Ferreira, P. B. de Camargo, A. C. L. da Costa, B. J. Enquist, S. R. Saleska, Isoprene emission structures tropical tree biogeography and community assembly responses to climate. *New Phytol.* **220**, 435–446 (2018). doi:10.1111/nph.15304 Medline

38. L. S. Leigh, T. Burgess, B. D. Marino, Y. D. Wei, Tropical rainforest biome of Biosphere 2: Structure, composition and results of the first 2 years of operation. *Ecol. Eng.* **13**, 65–93 (1999). doi:10.1016/S0925-8574(98)00092-5

39. B. Osmond, G. Ananyev, J. Berry, C. Langdon, Z. Kolber, G. Lin, R. Monson, C. Nichol, U. Rascher, U. Schurr, S. Smith, D. Yakir, Changing the way we think about global change research: Scaling up in experimental ecosystem science. *Glob. Change Biol.* **10**, 393–407 (2004). doi:10.1111/j.1529-8817.2003.00747.x

40. E. Pegoraro, L. Abrell, J. Van Haren, G. Barron-Gafford, K. A. Grieve, Y. Malhi, R. Murthy, G. Lin, The effect of elevated atmospheric CO2 and drought on sources and sinks of isoprene in a temperate and tropical rainforest mesocosm. *Glob. Change Biol.* **11**, 1234–1246 (2005). doi:10.1111/j.1365-2486.2005.00986.x

41. E. Pegoraro, A. Rey, L. Abrell, J. Vanharen, G. H. Lin, Drought effect on isoprene production and consumption in Biosphere 2 tropical rainforest. *Glob. Change Biol.* **12**, 456–469 (2006). doi:10.1111/j.1365-2486.2006.01112.x

42. J. Evaristo, M. Kim, J. Haren, L. A. Pangle, C. J. Harman, P. A. Troch, J. J. McDonnell, Characterizing the Fluxes and Age Distribution of Soil Water, Plant Water, and Deep Percolation in a Model Tropical Ecosystem. *Water Resour. Res.* **55**, 3307–3327 (2019). doi:10.1029/2018WR023265

43. J. L. M. van Haren, L. L. Handley, K. Y. Biel, V. N. Kudeyarov, J. E. T. McLain, D. A. Martens, D. C. Colodner, Drought-induced nitrous oxide flux dynamics in an enclosed tropical forest. *Glob. Change Biol.* **11**, 1247–1257 (2005). doi:10.1111/j.1365-2486.2005.00987.x

44. H. J. Scott, Characteristics of soils in the tropical rainforest biome of Biosphere 2 after 3 years. *Ecol. Eng.* **13**, 95–106 (1999). doi:10.1016/S0925-8574(98)00093-7

45. M. Finn, The mangrove mesocosm of Biosphere 2: Design, establishment and preliminary results. *Ecol. Eng.* **6**, 21–56 (1996). doi:10.1016/0925-8574(95)00050-X

46. P. F. Scholander, E. D. Bradstreet, E. A. Hemmingsen, H. T. Hammel, Sap Pressure in Vascular Plants: Negative hydrostatic pressure can be measured in plants. *Science* **148**, 339–346 (1965). doi:10.1126/science.148.3668.339 Medline

47. D. J. Barrett, J. T. Hatton, J. E. Ash, M. C. Ball, Evaluation of the heat pulse velocity technique for measurement of sap flow in rainforest and eucalypt forest species of south-eastern Australia. *Plant Cell Environ.* **18**, 463–469 (1995). doi:10.1111/j.1365-3040.1995.tb00381.x

48. F. C. Meinzer, B. J. Bond, J. M. Warren, D. R. Woodruff, Does water transport scale universally with tree size? *Funct. Ecol.* **19**, 558–565 (2005). doi:10.1111/j.1365-2435.2005.01017.x

49. S. D. Wullschleger, A. W. King, Radial variation in sap velocity as a function of stem diameter and sapwood thickness in yellow-poplar trees. *Tree Physiol.* **20**, 511–518 (2000). doi:10.1093/treephys/20.8.511 Medline

50. T. Gebauer, V. Horna, C. Leuschner, Variability in radial sap flux density patterns and sapwood area among seven co-occurring temperate broad-leaved tree species. *Tree Physiol.* **28**, 1821–1830 (2008). doi:10.1093/treephys/28.12.1821 Medline

51. M. Altaf Arain, W. James Shuttleworth, B. Farnsworth, J. Adams, O. Lutfi Sen, Comparing micrometeorology of rain forests in Biosphere-2 and Amazon basin. *Agric. For. Meteorol.* **100**, 273–289 (2000). doi:10.1016/S0168-1923(99)00153-7

52. L. A. Pangle, S. B. DeLong, N. Abramson, J. Adams, G. A. Barron-Gafford, D. D. Breshears, P. D. Brooks, J. Chorover, W. E. Dietrich, K. Dontsova, M. Durcik, J. Espeleta, T. P. A. Ferre, R. Ferriere, W. Henderson, E. A. Hunt, T. E. Huxman, D. Millar, B. Murphy, G.-Y. Niu, M. Pavao-Zuckerman, J. D. Pelletier, C. Rasmussen, J. Ruiz, S. Saleska, M. Schaap, M. Sibayan, P. A. Troch, M. Tuller, J. van Haren, X. Zeng, The Landscape Evolution Observatory: A large-scale controllable infrastructure to study coupled Earth-surface processes. *Geomorphology* **244**, 190–203 (2015). doi:10.1016/j.geomorph.2015.01.020

53. A. L. Buck, New Equations for Computing Vapor Pressure and Enhancement Factor. *J. Appl. Meteorol.* **20**, 1527–1532 (1981). doi:10.1175/1520-0450(1981)020<1527:NEFCVP>2.0.CO;2

54. L. Fasbender, A. M. Yáñez-Serrano, J. Kreuzwieser, D. Dubbert, C. Werner, Real-time carbon allocation into biogenic volatile organic compounds (BVOCs) and respiratory carbon dioxide (CO2) traced by PTR-TOF-MS, 13CO2 laser spectroscopy and 13C-pyruvate labelling. *PLOS ONE* **13**, e0204398 (2018). doi:10.1371/journal.pone.0204398 Medline

55. J. de Gouw, C. Warneke, T. Karl, G. Eerdekens, C. van der Veen, R. Fall, Sensitivity and specificity of atmospheric trace gas detection by proton-transfer-reaction mass spectrometry. *Int. J. Mass Spectrom.* **223-224**, 365–382 (2003). doi:10.1016/S1387-3806(02)00926-0

56. R. Holzinger, PTRwid: A new widget tool for processing PTR-TOF-MS data. *Atmos. Meas. Tech.* **8**, 3903–3922 (2015). doi:10.5194/amt-8-3903-2015

57. J. de Gouw, C. Warneke, Measurements of volatile organic compounds in the earth's atmosphere using proton-transfer-reaction mass spectrometry. *Mass Spectrom. Rev.* **26**, 223–257 (2007). doi:10.1002/mas.20119 Medline

58. R. Holzinger, W. J. F. Acton, W. J. Bloss, M. Breitenlechner, L. R. Crilley, S. Dusanter, M. Gonin, V. Gros, F. N. Keutsch, A. Kiendler-Scharr, L. J. Kramer, J. E. Krechmer, B. Languille, N. Locoge, F. Lopez-Hilfiker, D. Materić, S. Moreno, E. Nemitz, L. L. J. Quéléver, R. Sarda Esteve, S. Sauvage, S. Schallhart, R. Sommariva, R. Tillmann, S. Wedel, D. R. Worton, K. Xu, A. Zaytsev, Validity and limitations of simple reaction kinetics to calculate concentrations of organic compounds from ion counts in PTR-MS. *Atmos. Meas. Tech.* **12**, 6193–6208 (2019). doi:10.5194/amt-12-6193-2019

59. J. M. Zobitz, J. P. Keener, H. Schnyder, D. R. Bowling, Sensitivity analysis and quantification of uncertainty for isotopic mixing relationships in carbon cycle research. *Agric. For. Meteorol.* **136**, 56–75 (2006). doi:10.1016/j.agrformet.2006.01.003

60. J. Pinheiro, D. Bates, S. DebRoy, D. Sakar, R Core Team, nlme: Linear and Nonlinear Mixed Effects Models. R package version 3.1-152 (2021).

61. S. Wood, *Generalized Additive Models: An Introduction with R* (CRC Press, 2006).